



PAPER • OPEN ACCESS

A practical guide to electromagnetically induced transparency in atomic vapor

To cite this article: Ran Finkelstein *et al* 2023 *New J. Phys.* **25** 035001

View the [article online](#) for updates and enhancements.

You may also like

- [Biomedical applications of electrical impedance tomography](#)
Richard H Bayford and Bill R B Lionheart
- [10th International Conference on Electrical Impedance Tomography \(The University of Manchester, UK, 15–19 June 2009\)](#)
Richard Bayford and Bill Lionheart
- [Some reflections on the EIT Conference \(London, UK, 22–24 June 2005\)](#)
Theo J C Faes, Huib R van Genderingen and Anton Vonk Noordegraaf

**PAPER**

A practical guide to electromagnetically induced transparency in atomic vapor

OPEN ACCESS**RECEIVED**

21 September 2022

REVISED

13 December 2022

ACCEPTED FOR PUBLICATION



15 February 2023

PUBLISHED

7 March 2023

Original Content from
this work may be used
under the terms of the
[Creative Commons
Attribution 4.0 licence](#).

Any further distribution
of this work must
maintain attribution to
the author(s) and the title
of the work, journal
citation and DOI.

Ran Finkelstein^{1,2} , Samir Bali³, Ofer Firstenberg¹  and Irina Novikova^{4,*}¹ Department of Physics of Complex Systems, Weizmann Institute of Science, Rehovot 7610001, Israel² Division of Physics, Mathematics and Astronomy, California Institute of Technology, Pasadena, CA 91125, United States of America³ Department of Physics, Miami University, Oxford, OH 45056, United States of America⁴ Department of Physics, William and Mary, Williamsburg, VA 23187, United States of America

* Author to whom any correspondence should be addressed.

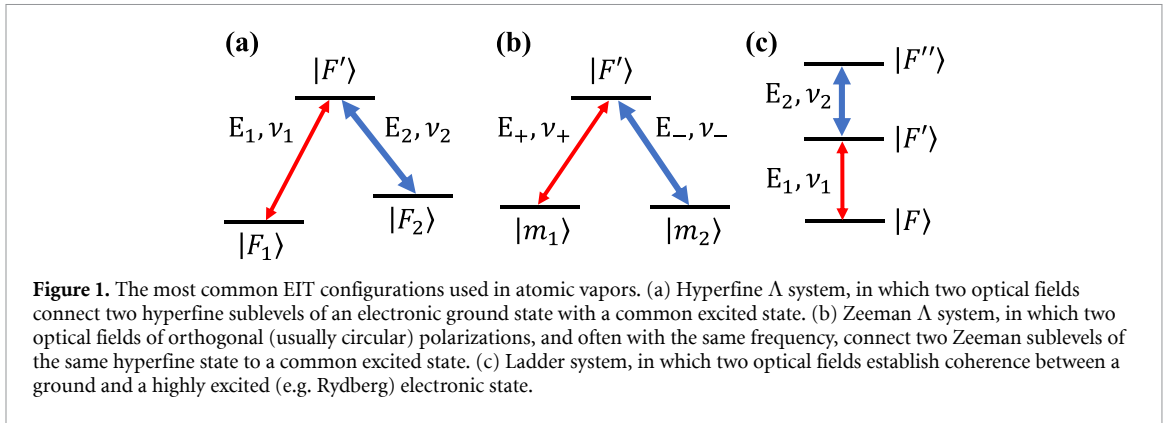
E-mail: inovikova@physics.wm.edu**Keywords:** tutorial, EIT, quantum optics**Abstract**

This tutorial introduces the theoretical and experimental basics of electromagnetically induced transparency (EIT) in thermal alkali vapors. We first give a brief phenomenological description of EIT in simple three-level systems of stationary atoms and derive analytical expressions for optical absorption and dispersion under EIT conditions. Then we focus on how the thermal motion of atoms affects various parameters of the EIT system. Specifically, we analyze the Doppler broadening of optical transitions, ballistic versus diffusive atomic motion in a limited-volume interaction region, and collisional depopulation and decoherence. Finally, we discuss the common trade-offs important for optimizing an EIT experiment and give a brief ‘walk-through’ of a typical EIT experimental setup. We conclude with a brief overview of current and potential EIT applications.

1. Introduction

Electromagnetically induced transparency (EIT) [1, 2] may be described almost like a magic tool: it makes opaque objects transparent and slows down light pulses to a crawl, even trapping these light pulses inside material objects. These make it a fun topic for public lectures, but more importantly in the last decades it has inspired a myriad of new applications, from precise atomic clocks and magnetometers [3, 4] to quantum information tools [5–8]. In terms of its importance for atomic, molecular, and optical physics, the introduction of the concept of EIT may be compared with the demonstration of optical pumping several decades earlier [9]. Optical pumping gave physicists the ability to control atomic populations by means of optical fields. Similarly, EIT extended this control into the realm of coherent superpositions and quantum states and, in parallel, allows for manipulation of light by atoms, ushering a new approach for realization of strong light-atom coupling using collective enhancement [10–12]. Unlike the standard quantum electrodynamics (QED) single-atom approach that requires strong coupling of an individual atom to a photonic mode, here the strong coupling is due to the collective enhancement provided by the large ensemble of identical atoms [11, 13, 14]. No high-quality cavity is required, and the resulting collective atomic state is very robust and can faithfully preserve quantum information originally carried by the optical probe.

The essence of the EIT effect is the strong coupling of a (usually weak) optical probe field to a long-lived excitation of an emitter by means of another, strong control field. The resulting two-photon transitions give optical access to high-Q quantum superpositions while avoiding optical losses associated with individual optical transitions. The term ‘electromagnetically induced transparency’ became widely used after its introduction in 1991 [15], although the essential concept was first described a few years earlier [16], and its more humble incarnation—coherent population trapping (CPT)—was known since 1975 and had been explored for metrological applications [17, 18]. By now, EIT has been studied in a broad range of physical systems: atoms, molecules, ions, plasmas, crystals, plasmons, etc [19–21]. In atoms, EIT typically utilizes two-photon transitions between two spin states of the same electronic level or between ground and highly



excited electronic states in, correspondingly, Λ and ladder configurations, shown in figure 1. In principle, EIT can be also observed in a V scheme, in which two excited states are connected to a common ground state. However, this configuration does not offer much advantage for atomic systems [22] and is typically explored for other platforms [19, 23]. While narrow transparency resonances can be observed in both cold and hot atoms, thermal motion in atomic vapor adds a new dimension to the EIT treatment and results in additional restrictions or opportunities, depending on the situation.

In this paper, we focus on the properties of EIT in thermal vapors of alkali metals. One of the key advantages of such a platform is its simplicity: while a typical cold atom apparatus requires a vacuum system and additional infrastructure for cooling and trapping atoms, atomic vapor can be contained in an evacuated transparent cell with a simple heater to control atomic vapor density. This simplicity gives vapor cell-based EIT experiments great flexibility to adapt to the requirements of different applications. For example, chip-scale vapor cells and vapor-filled fibers and waveguides enable the development of compact EIT-based tools and photonic elements [24]. It is also usually fairly straightforward to isolate a vapor cell from environmental perturbations (for example, placing a cell inside a magnetic shield efficiently suppresses stray magnetic fields). At the same time, the cell itself can be designed so as not to disturb its magnetic or electric environment, a desirable property for non-invasive sensors [25, 26]. Of course, atomic motion introduces several important restrictions to the experimental arrangement—but we will save those for later discussion as detailed below.

This paper is organized as follows: section 2 introduces the basic framework for describing EIT and discusses its basic properties. Section 3 discusses the effects of atomic motion on EIT. Section 4 discusses important considerations and trade-offs of an atomic vapor-based EIT experiment, while section 5 provides practical recommendations for EIT experimental realizations. Finally, section 6 gives a brief overview of basic EIT applications.

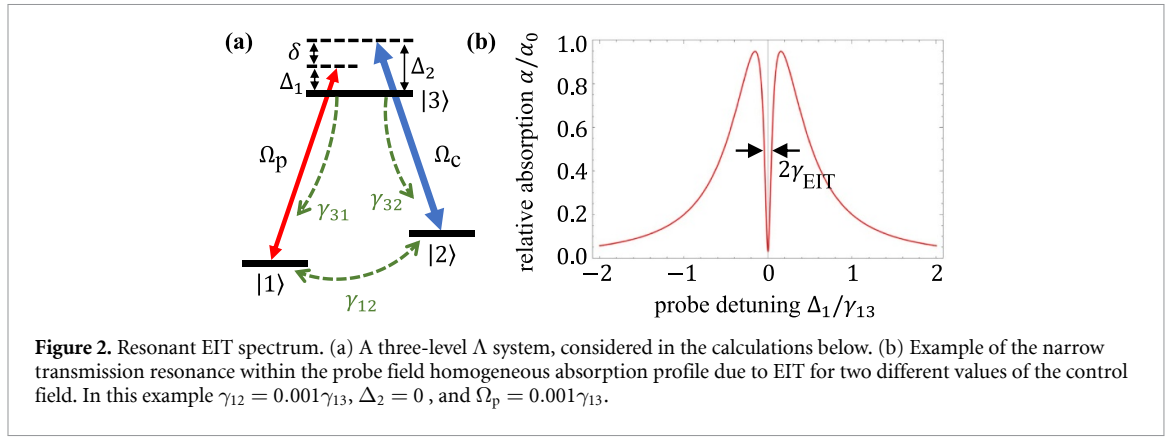
2. EIT: concept and basic properties

2.1. Dark state

There are several ways to explain EIT, but probably the most intuitive one involves the introduction of a so-called ‘dark state’ - a quantum superposition of the atomic levels that does not interact with both laser fields. A traditional EIT arrangement includes a three-level atomic (or atom-like) system, in which two of the levels are coupled to the common third level via two near-resonant electromagnetic fields, as shown in figure 1. Assuming that each optical field interacts with only its corresponding transition, the interaction Hamiltonian for such system can be written as

$$\hat{H} = \begin{pmatrix} -\hbar\omega_{13} & 0 & -\mu_{13}E_1 \\ 0 & -\hbar\omega_{23} & -\mu_{23}E_2 \\ -\mu_{13}E_1 & -\mu_{23}E_2 & 0 \end{pmatrix}, \quad (1)$$

where ω_{13} and ω_{23} are the frequency of the corresponding atomic transitions (here we assumed the energy of the state $|3\rangle$ to be zero), $E_{1,2} = \tilde{E}_{1,2}\exp(-i\nu_{1,2}t) + c.c.$ are the electromagnetic fields interacting with each atomic transition, and μ_{ij} is the dipole moment of the corresponding atomic transition. Since we will be mostly interested in the steady-state or slowly varying atomic evolution, we can apply the rotating wave approximation and remove all fast oscillating terms. Under this approximation, and moving to a frame rotating at the fields’ frequencies, the Hamiltonian \hat{H} can be rewritten as



$$\hat{H}_R = \begin{pmatrix} -\hbar\Delta_1 & 0 & -\mu_{13}\tilde{E}_1 \\ 0 & -\hbar\Delta_2 & -\mu_{23}\tilde{E}_2 \\ -\mu_{13}\tilde{E}_1^* & -\mu_{23}\tilde{E}_2^* & 0 \end{pmatrix}. \quad (2)$$

Here, $\Delta_i = \nu_i - \omega_{i3}$ is the one-photon detuning of each laser from its corresponding atomic transition.

A peculiar property of such a Hamiltonian is the existence of a zero-eigenvalue eigenstate, such that $\hat{H}_R|D\rangle = 0$. This state is thus decoupled from the interactions with the optical fields. In the following discussion we focus on a Λ interaction scheme, shown in figure 2, since its dark state involves two long-lived ground states, typically resulting in the most dramatic modification of the optical properties. However, all the procedures are very similar for other schemes. Also, in the majority of experiments one optical field is used as a probe of atomic properties, while the other serves mainly for control purposes; thus, we will use the ‘probe’ and ‘control’ nomenclature here to describe the two optical fields, and define their Rabi frequencies as $\Omega_p = \mu_{13}\tilde{E}_1/\hbar$ and $\Omega_c = \mu_{23}\tilde{E}_2/\hbar$, correspondingly.

It is easiest to find $|D\rangle$ for the resonant conditions, in which each laser is tuned exactly on resonance $\nu_1 = \omega_{13}$ and $\nu_2 = \omega_{23}$, i.e. $\Delta_1 = \Delta_2 = 0$, although it exists even for non-zero laser detunings. Notably, $|D\rangle$ is a superposition of only two atomic states $|1\rangle$ and $|2\rangle$:

$$|D\rangle = (\Omega_p|2\rangle - \Omega_c|1\rangle)/\Omega, \quad (3)$$

where $\Omega = \sqrt{|\Omega_p|^2 + |\Omega_c|^2}$. It is also important to note that a dark state exists for any three-level configuration, regardless of exact values of relative energies of the chosen atomic states or the strengths of the optical fields, down to the single-photon level in a fully quantum EIT treatment [27]. In case of strong control and weak probe fields ($\Omega_p \ll \Omega_c$), most of the atoms will still be found in the state $|1\rangle$, similar to the case of incoherent optical pumping. That is one of the fascinating features of the dark state: if atoms are definitely in the state $|1\rangle$ they strongly absorb the probe field; however, when in a dark state they become ‘invisible’, leading (in principle) to a complete transparency, even though they are still *mostly* in the same state $|1\rangle$.

To take full advantage of the EIT effect, the levels are chosen such that the states $|1\rangle$ and $|2\rangle$ have a longer lifetime than the state $|3\rangle$. Especially in the Λ configuration, the first two states are chosen among the ground states manifold. In this case, an atom in the dark state cannot be promoted into the electronic excited states, prohibiting the fluorescence and making the atom ‘dark’ to an external observer (which is historically the origin of the term ‘dark state’ [17]). At the same time, the absence of the spontaneous emission removes the dominant optical loss mechanism, so the laser fields can traverse the resonant atomic medium without any absorption—experiencing the transparency induced by the presence of a control electromagnetic field.

By analogy to the ‘dark state’, we can introduce an orthogonal ‘bright’ superposition $|B\rangle = (\Omega_p^*|1\rangle + \Omega_c^*|2\rangle)/\Omega$ that is coupled to the excited state $|3\rangle$, so that the interaction Hamiltonian (for $\Delta_1 = \Delta_2 = 0$) may be written as

$$\hat{H}_R = -\hbar\Omega(|3\rangle\langle B| + |B\rangle\langle 3|). \quad (4)$$

It is easy to see that the relative phase of the atomic superposition is critical to ensure the non-interaction condition for the dark state. For example, if the phase of one of the fields is suddenly flipped by π , thus changing the minus sign in the dark state to plus, the atoms temporarily become absorbing, until the atomic coherence is adjusted to the new conditions [28]. Using this argument, we can qualitatively explain the spectral width of the EIT resonance, although accurate derivation requires the density-matrix formalism described in the next subsection.

Above, we specifically assumed that the frequencies of each optical field match exactly the frequencies of the corresponding transitions. One can show that even for non-zero laser detunings $\Delta_{1,2}$, the steady-state dark state of equation (3) exists for the zero two-photon detuning $\delta = 0$, where we define $\delta = \Delta_1 - \Delta_2 = \nu_1 - \nu_2 - \omega_{12}$ as the mismatch between the two-photon transition frequency and the frequency difference between states $|1\rangle$ and $|2\rangle$. If a small non-zero two-photon detuning δ is introduced, the state of atoms initially prepared in $|D\rangle$ evolves in time as

$$|D_\delta(t)\rangle = (\Omega_p|2\rangle - e^{i\delta \cdot t}\Omega_c|1\rangle) / \Omega, \quad (5)$$

causing the sign of the dark-state phase to slowly change. Since in reality atoms cannot maintain their coherence forever, the dark state can exist only for a finite lifetime τ_{coh} . So if the two-photon detuning is small, such that the accumulated phase $\delta \cdot \tau_{\text{coh}}$ is negligible, the dark state stays largely non-interacting, and EIT is preserved. But as detuning increases, the effect of the phase evolution becomes more pronounced. In fact, we can roughly estimate the spectral EIT width to be inversely proportional to the dark-state lifetime by setting $\delta \cdot \tau_{\text{coh}} \approx \pi/2$. Such an estimate is quite accurate in the limit of very weak optical fields. We can also use this model to qualitatively explain the so-called power-broadening effect: the increase of the EIT linewidth with the power of the optical fields. Equation (5) assumes free evolution of the atomic state, which works well for weak optical fields; the stronger the fields are, the larger is the probability that the evolving state is rephased by the repeated interaction, thus attenuating the free phase evolution and consequently increasing the transparency tolerance to non-zero detuning.

2.2. Note on terminology: CPT vs EIT vs Raman

One of the difficulties with a literature search on EIT-related research is the different terminology used. For example, the two-photon transmission resonances can be referred to as EIT, CPT, dark resonances, and Raman resonances. Moreover, different people sometimes put slight differentiation between each of these terms, so here we outline what we perceive as the most common definitions.

CPT is often referred to as the experimental arrangement involving a Λ -system with two long-lived energy levels (typically two hyperfine or Zeeman ground state sublevels) and two optical fields of comparable strength. In this case atoms are ‘trapped’ in a quantum superposition with near-maximum coherence, a process which can be considered as a generalization of the optical pumping process. Such a configuration is most common for metrology applications, such as CPT-based atomic clocks, magnetometers, etc [3, 4].

EIT then is a more general case in which the transmission of a resonant optical field is enhanced by means of another optical field, particularly without any reduction of the atomic population in the initial atomic state. This effect can be realized in any three-level system, and, in principle, for arbitrary values of the optical fields. However, most often EIT experiments imply a strong control optical field Ω_c and a weak probe optical field Ω_p . In this arrangement, EIT looks the most ‘counterintuitive’, especially in the ladder system, where adding a strong control field between nominally empty excited states changes the probe absorption dramatically without noticeably changing atomic populations. Indeed, according to the dark-state equation (3), for $\Omega_p \ll \Omega_c$, the population of the state $|1\rangle$, coupled to the weaker optical field, is $|\Omega_c^2| / (|\Omega_c^2| + |\Omega_p^2|) \approx 1$. This regime is most relevant to quantum information applications, in which EIT is used for realization of the strong coupling between quantum optical fields (particularly, single photons) and long-lived atomic states, e.g. for slow light and quantum memory [12].

EIT is of course a small subset of general two-photon Raman processes. However, in the context of light-atom interaction, Raman resonances often refer to the case of narrow absorption resonances appearing in a Λ system when the two optical fields are detuned from the excited state, while maintaining the two-photon resonance (we will consider the effect of the laser detuning on EIT below). In the last decade, such far-detuned Raman resonances became a viable alternative to EIT for quantum memory applications [29].

2.3. Density matrix description of the EIT

While the concept of the dark state provides an intuitive insight into the nature of EIT, the accurate description of this process requires proper account of the decoherence processes for both optical transitions and, more importantly, the atomic coherence associated with the dark state. Since the wave-function formalism is not adequate for describing quantum systems in the presence of decoherence, we shall utilize the density matrix formalism. In this formalism, the evolution of the atomic state matrix $\hat{\rho}$ under the action of the Hamiltonian \hat{H}_R , is described by the Maxwell–Bloch equation [30]

$$\frac{d\hat{\rho}}{dt} = -\frac{i}{\hbar} [\hat{H}_R, \hat{\rho}] + \mathcal{L}_\Gamma[\hat{\rho}], \quad (6)$$

where the superoperator \mathcal{L}_Γ encompasses all the decoherence effects. We will discuss the specific decoherence effects associated with various aspects of the environment [31] in detail in section 3. For now we introduce the general decoherence rates phenomenologically: γ_i is the population decay rate of the i th state (in case of a state having more than one decay channel, r_{ij} is the branching ratio to the state j), and γ_{ij} is the decoherence rate of the corresponding off-diagonal matrix element ρ_{ij} . Here we will also assume a closed system (i.e., there is no population exchange outside of the three atomic levels), although it has been shown that the corresponding calculations for the open system result in a very similar outcome [32]. Finally, since the Λ system, shown in figure 2, is the more common EIT configuration, in the following we will assume that the states $|1\rangle$ and $|2\rangle$ are sublevels of the ground electronic state hence experience no spontaneous emission, and are both coupled to the common excited electronic state $|3\rangle$. In this case, the time evolution equations for the density matrix elements are

$$\begin{aligned}\dot{\rho}_{11} &= r_{31}\gamma_3 - i\Omega_p\rho_{13} + i\Omega_p^*\rho_{31} \\ \dot{\rho}_{22} &= r_{32}\gamma_3 - i\Omega_c\rho_{23} + i\Omega_c^*\rho_{32} \\ \rho_{33} &= 1 - \rho_{11} - \rho_{22} \\ \dot{\rho}_{21} &= -(\gamma_{12} - i\delta)\rho_{21} - i\Omega_p\rho_{23} + i\Omega_c^*\rho_{31} \\ \dot{\rho}_{31} &= -(\gamma_{13} - i\Delta_1)\rho_{31} + i\Omega_c\rho_{21} + i\Omega_p(\rho_{11} - \rho_{33}) \\ \dot{\rho}_{32} &= -(\gamma_{23} - i\Delta_2)\rho_{32} + i\Omega_p\rho_{12} + i\Omega_c(\rho_{22} - \rho_{33}).\end{aligned}\quad (7)$$

These equations can provide the exact solution for any values of experimental parameters, but in general can only be solved numerically. In this section we will consider only the steady-state solution to analyze the main characteristics of the EIT transmission resonances. Even then, though equation (7) become a system of linear equations and can be solved analytically, the resulting expressions are rather cumbersome. So here we analyze the most common case of a strong control field and a weak probe field $\Omega_p \ll \Omega_c$, in which the system's response to the probe field is linear.

In the weak-probe regime, it is convenient to use the perturbative approach to the solution, keeping only the linear terms in Ω_p . To zeroth-order approximation, we can assume that all atomic population is optically pumped into the state $|1\rangle$ (assuming that the control field is sufficiently strong to provide efficient optical pumping): $\rho_{11}^{(0)} = 1$, and $\rho_{22}^{(0)} = \rho_{33}^{(0)} = 0$. Also $\rho_{23}^{(0)} = 0$, since this is the coherence between two empty states. Substituting these values into the right hand side of equation (7) and keeping only linear terms in Ω_p substantially simplifies the situation since only two equations remain:

$$\begin{aligned}0 &= -\Gamma_{12}\rho_{21} + i\Omega_c^*\rho_{31} \\ 0 &= -\Gamma_{13}\rho_{31} + i\Omega_c\rho_{21} + i\Omega_p,\end{aligned}\quad (8)$$

where we use $\Gamma_{12} = \gamma_{12} - i\delta$ and $\Gamma_{13} = \gamma_{13} - i\Delta_1$. This leads to very simple and elegant expressions for the ground state and optical coherences

$$\rho_{21} = -\frac{\Omega_p\Omega_c^*}{\Gamma_{12}\Gamma_{13} + |\Omega_c|^2}\quad (9)$$

$$\rho_{31} = i\Omega_p\frac{\Gamma_{12}}{\Gamma_{12}\Gamma_{13} + |\Omega_c|^2}.\quad (10)$$

Then the probe linear susceptibility χ_p of an ensemble of N atoms per unit volume is

$$\chi_p(\Delta_1, \delta) = \frac{N\mu_{13}^2}{\hbar\epsilon_0}\frac{\rho_{31}}{\Omega_p} = i\frac{N\mu_{13}^2}{\hbar\epsilon_0}\frac{\Gamma_{12}}{\Gamma_{12}\Gamma_{13} + |\Omega_c|^2}.\quad (11)$$

It is easy to see that, when no ground state coherence exists between the states $|1\rangle$ and $|2\rangle$, χ_p reverts back to its value for a two-level system $\chi_p^{(2\text{-level})}(\Delta_1) = i\frac{N\mu_{13}^2}{\hbar\epsilon_0\Gamma_{13}}$. It is convenient to define α_0 , the unsaturated resonant absorption coefficient (field absorption per unit length) in the absence of EIT, as:

$$\alpha_0 = k_p/2\chi_p^{(2\text{-level})}(0) = \frac{k_p N\mu_{13}^2}{2\hbar\epsilon_0\gamma_{13}},\quad (12)$$

where $k_p = 2\pi\nu_p/c$ is the probe field's wavevector in vacuum. Then, the susceptibility in equation (11) can be written as

$$\chi_p(\Delta_1, \delta) = i\alpha_0\frac{2\gamma_{13}}{k_p}\frac{\Gamma_{12}}{\Gamma_{12}\Gamma_{13} + |\Omega_c|^2}.\quad (13)$$

In the ideal case of no ground-state decoherence $\gamma_{12} = 0$ and zero two-photon detuning $\delta = 0$ (i.e., for $\Gamma_{12} = 0$), the susceptibility completely vanishes, resulting in 100% transparency for the probe field. This result is particularly counter-intuitive for resonant optical fields, as one expects the strongest resonant absorption due to large atomic population in the state $|1\rangle$. This is the origin of the name for EIT.

2.4. Near-resonant fields, EIT

Let us first consider the case of the probe laser tuned exactly to the atomic resonance $\Delta_1 = 0$ but allow a small two-photon detuning $\delta \ll \gamma_{13}$. In this case we can derive the canonical expression for the EIT susceptibility by substituting $\Gamma_{13} = \gamma_{13}$ and $\Gamma_{12} = \gamma_{13} - i\delta$ in equation (11):

$$\chi_p^{(\text{on-res.})}(\delta) = i\alpha_0 \frac{2}{k_p} \frac{[\gamma_{12}\gamma_{\text{EIT}} + \delta^2] - i\delta|\Omega_c|^2/\gamma_{13}}{\gamma_{\text{EIT}}^2 + \delta^2}, \quad (14)$$

where

$$\gamma_{\text{EIT}} = \gamma_{12} + |\Omega_c|^2/\gamma_{13}. \quad (15)$$

The absorption coefficient of the probe field in this case is

$$\alpha_p(\delta) = \alpha_0 \frac{\gamma_{12}\gamma_{\text{EIT}} + \delta^2}{\gamma_{\text{EIT}}^2 + \delta^2}. \quad (16)$$

At the exact two-photon resonance $\delta = 0$, the probe absorption is suppressed by the factor

$$\frac{\alpha_p(\delta = 0)}{\alpha_0} = \frac{\gamma_{12}}{\gamma_{\text{EIT}}} = \frac{\gamma_{12}}{\gamma_{12} + |\Omega_c|^2/\gamma_{13}}. \quad (17)$$

Realistically, we can approach almost complete transparency in the limit of the strong control field $|\Omega_c| \gg \sqrt{\gamma_{12}\gamma_{13}}$, resulting in the vanishing absorption suppression factor $\frac{\alpha_p(\delta=0)}{\alpha_0} = \frac{\gamma_{12}\gamma_{13}}{|\Omega_c|^2} \rightarrow 0$.

Equation (15) describes the linewidth of the EIT transmission resonance γ_{EIT} . It is easy to see that for a very weak control field, the resonance width is limited by the decoherence rate γ_{12} , which can in principle be very small, especially in the case of a Λ configuration. As the control power increases, the EIT resonance broadens proportionally. For most practical applications, the balance between such power broadening (a narrow resonance needs lower control power) and the absorption suppression factor (higher transmission needs higher control power) determines the optimal control field parameters. Not surprisingly, for many applications the optimal operation conditions correspond to the case when the power broadening term equals the natural decoherence term.

2.5. Off-resonant fields, EIT and Raman absorption

Let us now consider another limiting case in which the probe field is detuned relatively far away from the corresponding atomic transition, such that $\Delta_1 \gg \gamma_{13}$. To analyze the probe absorption for different control-field detunings, it is convenient to rewrite equation (11) as:

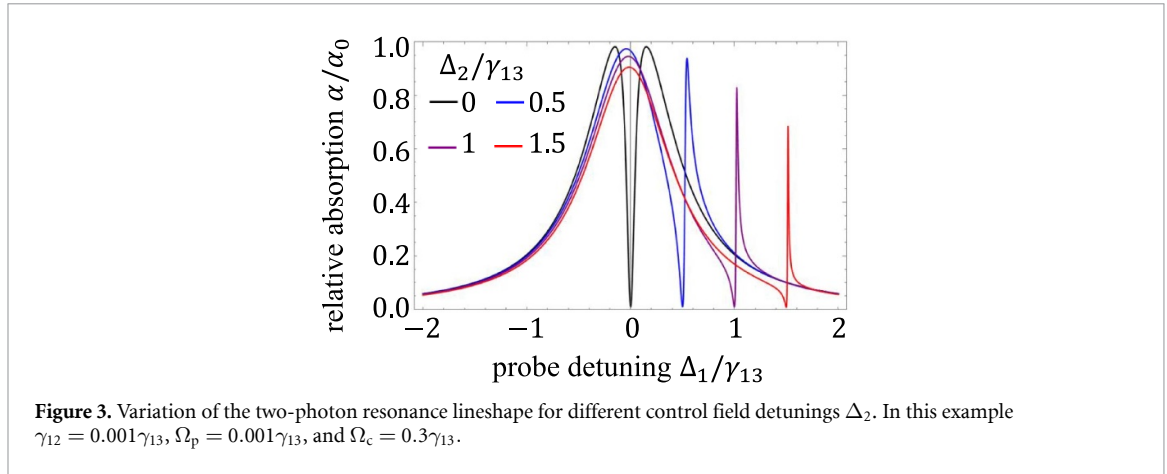
$$\chi_p^{(\text{off-res.})}(\Delta_1, \delta) = i\alpha_0 \frac{2\gamma_{13}}{k_p\Gamma_{13}} \left(1 - \frac{|\Omega_c|^2}{\Gamma_{12}\Gamma_{13} + |\Omega_c|^2} \right). \quad (18)$$

Here we can easily identify the first term as a resonant probe interaction, while the second term describes the control field effect. One can check that the largest relative contribution from the second term happens near the two-photon resonance $\delta \ll \Delta_1$. Then, taking into account $\Delta_1 \gg \gamma_{13}, \gamma_{12}$, we can simplify the expression for the off-resonant probe susceptibility as:

$$\chi_p^{(\text{off-res.})}(\Delta_1, \delta) \simeq i\alpha_0 \frac{2}{k_p} \frac{\gamma_{13}}{\gamma_{13} - i\Delta_1} + i\alpha_0 \frac{2}{k_p} \frac{|\Omega_c|^2/\Delta_1}{\gamma_R - i(\delta - \delta_R)}. \quad (19)$$

Here again the first term is the residual linear susceptibility, while the second term corresponds to a two-photon Raman absorption resonance with the width $\gamma_R = \gamma_{12} + \gamma_{13}|\Omega_c|^2/\Delta_1^2 \ll \gamma_{13}$, shifted from the exact two-photon resonance by $\delta_R = |\Omega_c|^2/\Delta_1$.

In the general case of the non-zero one-photon detuning, as shown in figure 3, the EIT resonance, which is symmetric when the probe field is tuned exactly to the optical transition, starts to become asymmetric with the laser detuning. Upon further increase of the one-photon detuning beyond the natural linewidth γ_{13} , the EIT feature transforms into a predominantly absorption resonance (albeit always accompanied by a



transparency feature at $\delta = 0$ as seen in figure 3). Throughout this transformation, the lineshape of the two-photon resonance can be well-described by a generalized Lorentzian:

$$\alpha(\delta) = \tilde{\gamma} \frac{A\tilde{\gamma} + B(\delta - \tilde{\delta})}{\tilde{\gamma}^2 + (\delta - \tilde{\delta})^2 + C}, \quad (20)$$

where all the parameters $A, B, C, \tilde{\gamma}, \tilde{\delta}$ are functions of the one-photon detuning Δ_1 . Analytical expressions for all of them straightforwardly follow from equation (11) and are calculated in [33, 34], but are rather cumbersome.

2.6. Ladder scheme and more complex systems

In the ladder EIT scheme, the probe field couples the ground state $|1\rangle$ to the excited state $|3\rangle$, and the strong control field is applied between the two excited states $|2\rangle$ and $|3\rangle$, as shown in figure 1(c). The general solution in this case is identical to that of the Λ scheme, with the main difference being that now the two-photon coherence ρ_{12} is between the ground and a highly excited state, and thus its decoherence rate is primarily driven by the radiative decay rate of the excited state γ_2 (and $\Gamma_{12} = \gamma_2/2 - i\delta$), where now the two-photon detuning is defined as $\delta = \Delta_1 + \Delta_2$. For that reason the ladder EIT is particularly powerful if the highly excited state has a long lifetime, which is the case for Rydberg states in alkali-metal atoms [35, 36].

Looking beyond a simple three-level system, one can generalize the expression for the probe linear susceptibility in the case of multiple atomic levels and multiple control fields, forming a chain of coupled states. It is easy to obtain an exact linear response for such a multi-level structure using the following prescription:

$$\chi_p = \alpha_0 \frac{\gamma}{\gamma - i\Delta + \sum_j \left(\text{nested} \right)_j}, \quad (21)$$

where

$$\left(\text{nested} \right)_j = \frac{|\Omega_j|^2}{\gamma_j - i\delta_j + \sum_k \left(\text{nested} \right)_{j,k}}, \text{ etc.}$$

Here each term in the summation \sum_j includes contributions from each control field Ω_j coupled to the same excited state as the probe field. If there are additional optical fields $\Omega_{j,k}$ linked through one of the ‘primary’ control fields Ω_j , their effect is included as the next ‘nested’ level, and so on.

An example of this procedure in action is given in figure 4 for a combined Λ and ladder configuration. In this configuration, two ‘primary’ control fields Ω_1 and Ω_2 are directly linked with the probe, and the ‘secondary’ control field $\Omega_{2,1}$ forms the additional nested resonance. Following the prescription above, one can easily find the probe susceptibility to be

$$\chi_p = \alpha_0 \frac{\gamma}{\gamma - i\Delta + \frac{|\Omega_1|^2}{\gamma_1 - i\delta_1} + \frac{|\Omega_2|^2}{\gamma_2 - i\delta_2 + \frac{|\Omega_{2,1}|^2}{\gamma_{2,1} - i\delta_{2,1}}}}. \quad (22)$$

2.8. EIT dynamics: slow and stored light

Up to now we have paid particular attention to the atomic absorption resonances. However, the corresponding spectral features in the refractive index are equally exciting. In particular, a power-dependent steep dispersion associated with narrow EIT resonances enables realization of controllable group velocity in a wide range from ‘slow’ to ‘fast’ light.

One can calculate the refractive index for the probe field using the real part of the susceptibility calculated in equation (11): $n = 1 + \text{Re}(\chi_p)$, although the general expression is rather cumbersome. To find the group velocity under the EIT conditions, however, we can neglect the one-photon detuning $\Delta_1 = 0$ and find the refractive index as a function of δ at the EIT peak

$$n(\delta) = 1 + \alpha_0 \frac{2\gamma_{13}}{k_p} \frac{\delta}{\gamma_{\text{EIT}}^2 + \delta^2} \frac{|\Omega_c|^2 - \gamma_{12}^2 - \delta^2}{\gamma_{13}^2}. \quad (26)$$

It is easy to see that exactly on resonance the refractive index is equal to one, but then varies rapidly with the two-photon detuning. In fact, it is possible to obtain the enhanced refractive index by tuning the lasers a little off the exact EIT resonance, while still taking advantage of the reduced absorption [39, 40].

The group velocity is determined by the slope of the dispersion curve, which is maximum at the EIT peak $\delta = 0$:

$$v_g = \frac{c}{n_g} = \frac{c}{1 + \nu_p \left. \frac{dn}{d\nu_p} \right|_{\delta=0}}. \quad (27)$$

Assuming $\delta \ll \Omega_c, \gamma_{13}$, we can find that the probe group velocity under the EIT conditions is determined by the strength of the control field,

$$v_g = \frac{c}{1 + \frac{c\alpha_0}{\pi\gamma_{13}} \frac{|\Omega_c|^2}{\gamma_{\text{EIT}}^2}}. \quad (28)$$

It is clear from equations (15) and (28) that by using a weaker control field, the group velocity can be reduced by many orders of magnitude compared to c . This regime is often referred to as ‘slow light’ and was demonstrated in 1999 in both cold and hot atoms [41–43]. The demonstrations of optical pulses propagating with speeds of a few tens of meters per second in both ultracold and hot atoms under EIT conditions attracted a lot of attention among scientists as well as the general population. Since then, this effect has been demonstrated in a wide variety of systems and has been considered for many applications. More detailed descriptions and experimental realizations of EIT-based slow light experiments in Rb vapor are discussed in [44–46].

Similarly, tuning to the bottom of the Raman absorption resonance can provide equally large but negative dispersion $dn/d\nu_p$, making the group velocity exceed the speed of light or even reach negative values (the ‘fast’ or ‘superluminal’ regime) [47]. The initial reports of the fast light observations [48], in which a pulse after interacting with atoms seemed to emerge ahead of its copy propagating in vacuum, initiated a lot of discussion regarding possible causality violation, as well as various definitions of speed with which information can be transferred in dispersive materials. Since then, the superluminal regime has been observed using both absorptive and gain resonances and has been proposed for improving the sensitivity of optical gyroscopes and white-light cavities [49].

Probably the most consequential EIT-related application is its role in development of quantum information technologies, and in particular quantum memories. Since two-photon interaction allows strong coupling between a weak optical field and a long-lived atomic coherence, mediated by the strength of a strong control field, the dynamic variation of this field allows reversible mapping of the quantum state of the probe field onto the collective quantum state of the atomic ensemble, and vice versa [50–52].

The detailed discussion of quantum memory operation is beyond the scope of this manuscript [12] and is the subject of several in-depth reviews [7, 53, 54]. To describe the basic principle of operation for the EIT quantum memory, it is convenient to think of the propagating probe optical field and the atomic ensemble as a single quasi-particle (often referred to as a ‘dark state polariton’, or DSP) consisting of coupled photonic and atomic components [11]. The ratio between the two is determined by the group velocity and, correspondingly, by the strength of the control optical field Ω_c . Weaker Ω_c reduces the group velocity, as predicted in equation (28), and increases the ‘weight’ of the atomic component of the DSP. A sudden reduction of the control field to zero arrests the DSP motion, forcing it to convert completely into atomic coherence. The quantum information is thus stored in the atomic memory for times shorter than the polariton lifetime, which can reach up to seconds for the case of atomic ground-state spin states. This information can then be read-out on-demand by simply restoring the control field, reactivating the DSP

motion. Many experiments have demonstrated the effectiveness of such quantum memory for storing quantum optical information carried by probe photon number, polarization, optical angular momentum, and more [7, 53, 54].

Another important aspect of atoms' ability to preserve quantum information is that it enables light-atom entanglement that is proven to be a crucial step in the development of a quantum repeater—a critical element for long-distance quantum communication. The first proposal for a practical quantum repeater [55] used spontaneous off-resonant Raman scattering to simultaneously produce a heralding photon and a correlated collective atomic excitation that can be later converted on-demand into a second photon via EIT-based control field read-out. This process thus produces a pair of entangled photons with controllable time interval that can be used to establish and extend the entanglement between neighboring nodes of a quantum network with beneficial resource scaling for longer distances. At the same time, this mechanism can also be used to realize an on-demand single photon source.

3. EIT in atomic vapor

Having presented the basics of EIT for stationary atoms, we now discuss the effects of thermal atomic motion. This motion, due to the atoms' high kinetic energy, is arguably the most prominent characteristic of thermal vapor. It results in a time-dependent interaction with the light fields, which is manifested as spectral broadening in the frequency domain or as decoherence in the time domain. To evaluate the importance of different motional effects, one should consider the time of flight T of an atom through the different length scales l in the problem. For example, l might be the wavelength of the excitation fields or the size of a finite excitation volume. The resulting spectral broadening is then given by

$$\sigma \simeq 1/T. \quad (29)$$

Generally, $T \propto l$ for ballistic motion, and $T \propto l^2$ for diffusive motion (as in a random walk).

Atomic motion affects the EIT lineshape via both 'one-photon' and 'two-photon' contributions [56]. The one-photon contribution refers to spectral broadening and decoherence of the $|1\rangle - |3\rangle$ transition, associated with the optical coherence ρ_{13} . This broadening is always present in vapor media, and, while it does not affect the EIT linewidth in principle, it acts to attenuate the absorption cross-section of the media. This attenuation results in a reduced optical depth. The two-photon contribution pertains to the overall transition from state $|1\rangle$ to state $|2\rangle$, associated with the (spin) coherence ρ_{12} . Motional broadening and decoherence of this transition results in broadening of the EIT linewidth and in reduced contrast of the EIT susceptibility (both real and imaginary parts). In the following, we discuss the different regimes of atomic motion in thermal vapors, as illustrated in figure 5, and their consequences.

3.1. Motional effects for ballistically moving atoms in an infinite beam

We begin by considering very wide beams, ideally plane-wave fields, as illustrated in figure 5(a). For thermal atoms moving ballistically in such a field, the optical wavelength λ sets the only relevant length-scale for motional effects, and the corresponding time-scale is $T \simeq \lambda/v_{\text{th}}$, where v_{th} is the mean thermal velocity [the root-mean-square (rms) of the one-dimensional velocity distribution]. The general formula (29) then yields an estimate of $\sigma \simeq v_{\text{th}}/\lambda$ for the expected spectral broadening. This broadening, known as Doppler broadening, can be alternatively estimated from the Doppler shifts $\delta \rightarrow \delta - \vec{k} \cdot \vec{v}$ each atom experiences in its own reference frame. Here \vec{v} is the atom's velocity, \vec{k} is the wavevector ($|\vec{k}| = 2\pi/\lambda$), and δ is the detuning between the laser frequency and the atomic transition frequency. The Doppler shift results in an inhomogeneous spectral broadening when averaging over the different velocities in the ensemble or over the different wavevectors composing the field.

More precisely, we consider an ensemble of atoms moving in a dilute medium, such that velocity-changing collisions are scarce and the atomic velocities can be considered fixed. The atoms traverse a uniform field with a periodically-modulated phase along the field's propagation direction. Using the transit-time approach (equation (29)), the Doppler broadening can be evaluated by considering the time it takes an atom to cross $l = \lambda/(2\pi)$, i.e. one radian of the phase of the excitation field:

$$\sigma_{\text{Dop}} = \frac{v_{\text{th}}}{\lambda/2\pi} = v_{\text{th}}|\vec{k}|. \quad (30)$$

Typical thermal velocities are in the range $v_{\text{th}} = 100 - 300 \text{ m s}^{-1}$ at ambient temperature, and the optical wavelength is on the range of $0.3 - 1.5 \mu\text{m}$. Therefore, a typical width σ_{Dop} of the one-photon transition is a few hundreds of MHz. Alternatively, using the Doppler-shifts approach, the exact spectral broadening is

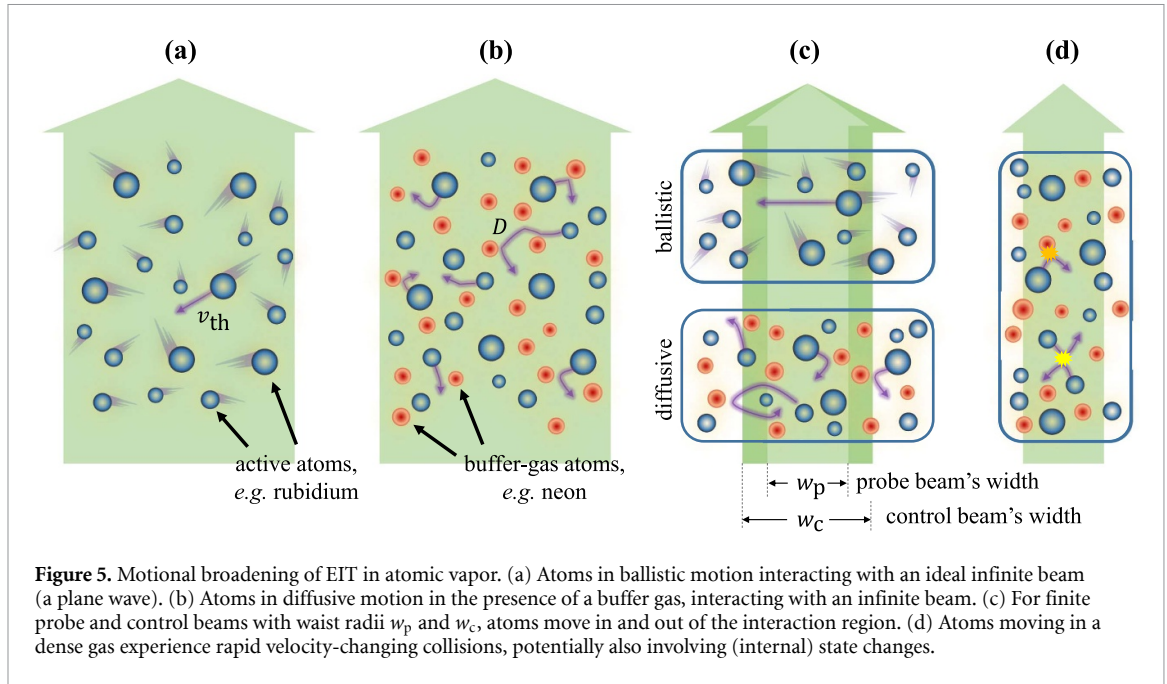


Figure 5. Motional broadening of EIT in atomic vapor. (a) Atoms in ballistic motion interacting with an ideal infinite beam (a plane wave). (b) Atoms in diffusive motion in the presence of a buffer gas, interacting with an infinite beam. (c) For finite probe and control beams with waist radii w_p and w_c , atoms move in and out of the interaction region. (d) Atoms moving in a dense gas experience rapid velocity-changing collisions, potentially also involving (internal) state changes.

obtained by summing over the atomic velocities, usually following the one-dimensional Maxwell–Boltzmann distribution

$$w(v) = \frac{1}{\sqrt{2\pi}v_{\text{th}}} e^{-v^2/2v_{\text{th}}^2}. \quad (31)$$

Assuming without loss of generality $\vec{k} \parallel \hat{z}$, the averaged susceptibility is given by

$$\chi_{\text{ensemble}}(\delta) = \int_{v_z=-\infty}^{\infty} \chi_p(\delta - kv_z)w(v_z)dv_z. \quad (32)$$

Therefore, the lineshape of the Doppler-broadened ensemble is a convolution of Lorentzian and Gaussian profiles, a spectrum known as a Voigt profile. A useful approximation to this profile is the pseudo-Voigt function, which is simply a linear combination of the Gaussian and the Lorentzian functions.

We now turn our focus to the EIT resonance. As EIT is a coherent two-photon process, it is dominated by the effective two-photon field $\Omega_c^* \Omega_p$. Atomic motion through this field, which has an effective two-photon wavevector $\vec{k}_{\text{eff}} = \vec{k}_p \pm \vec{k}_c$, governs the motional broadening of the EIT resonance. Here $(-)$ corresponds to a Λ level system and $(+)$ for a ladder system, i.e. depending on whether a photon is absorbed from or emitted into the control field during the excitation of the EIT spin wave. When the fields are similar in wavelength, one can choose the propagation direction of the control and probe (co-propagating or counter-propagating) such that \vec{k}_{eff} is small. In a Λ scheme there could be complete degeneracy (direction and frequency), such that $\vec{k}_{\text{eff}} = 0$. Often this degeneracy is lifted by assigning a slight angle of the control field relative to the probe field or by choosing two ground states with different energies due to applied magnetic field or hyperfine splitting. The small yet finite effective excitation wavelength is typically on the order of few cm^{-1} up to m^{-1} .

Figure 6 shows how EIT is maintained in an ensemble of atoms in thermal motion. Atoms at different velocities experience large one-photon Doppler shifts leading to an absorption linewidth of a few hundreds of MHz (grey shaded area). The absorption spectrum for each velocity group in the atomic ensemble features a doublet feature akin to Autler–Townes splitting. However, there is a narrow frequency region where none of the atomic velocity groups absorbs light. It is this region where the EIT line is formed, and thus all of the atomic velocity groups take part in the transparency formed. The power-broadened EIT linewidth is thus set by the inhomogeneous broadening of the excited state

$$\gamma_{\text{EIT}} = \frac{\Omega_c^2}{\sigma_{\text{Dop}}} + \gamma_{12}, \quad (33)$$

where σ_{Dop} is the one-photon Doppler width.

In a Ladder scheme, there is typically a large wavelength mismatch, and \vec{k}_{eff} cannot be made much smaller than the inverse of that residual wavelength, typically on the order of microns to hundreds of

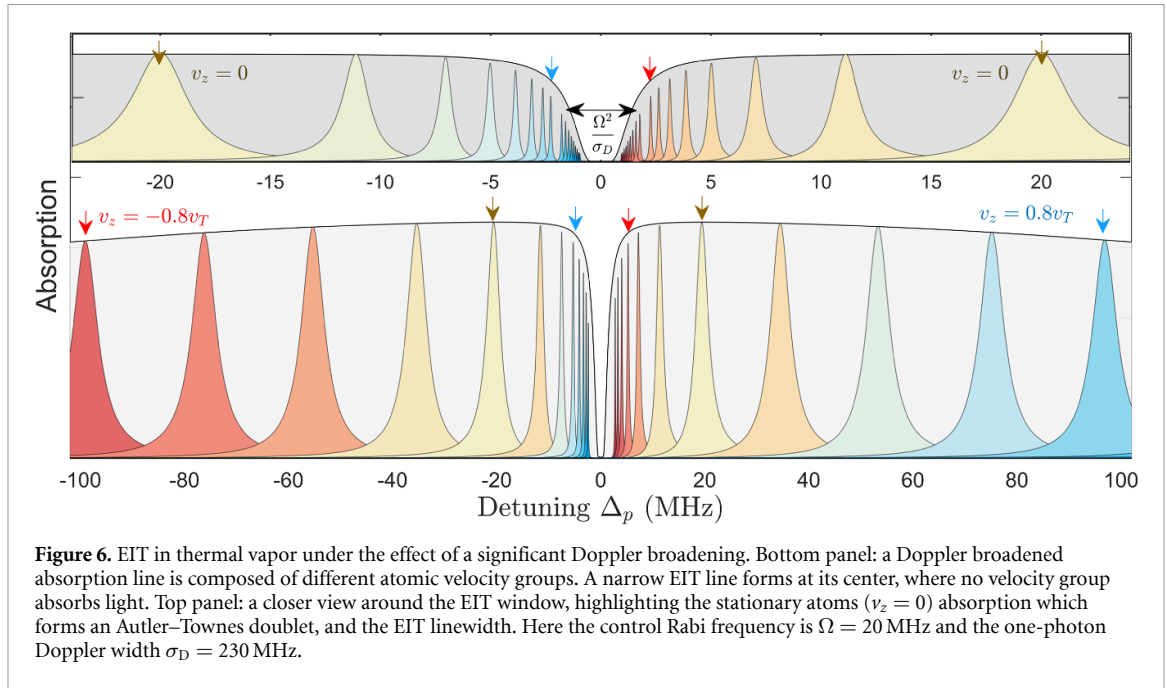


Figure 6. EIT in thermal vapor under the effect of a significant Doppler broadening. Bottom panel: a Doppler broadened absorption line is composed of different atomic velocity groups. A narrow EIT line forms at its center, where no velocity group absorbs light. Top panel: a closer view around the EIT window, highlighting the stationary atoms ($v_z = 0$) absorption which forms an Autler–Townes doublet, and the EIT linewidth. Here the control Rabi frequency is $\Omega = 20$ MHz and the one-photon Doppler width $\sigma_D = 230$ MHz.

microns. The Doppler shift of the EIT line for a given atomic velocity v is $\delta \rightarrow \delta - \vec{k}_{\text{eff}} \cdot \vec{v}$, which one can plug into the three-level susceptibility expression given by equation (14). The resulting broadening is known as Residual or two-photon Doppler broadening and is on the order of few MHz to tens of MHz for ladder-type systems. With a finite detuning from the intermediate state, such wavelength mismatch leads to a shift in the measured two-photon resonance, rather than just a broadening, as it inherently leads to a velocity-selective process [57]. Finally, we note that such motional dephasing is a special case of the general problem known as inhomogeneous dephasing. As such, it can in principle be reversed and eliminated [58].

3.2. Diffusive infinite beam

As we have seen, the ballistic motion of the atoms typically leads to substantial broadening and fast decoherence. A prominent solution to this problem in hot vapor is to add a relatively dense, inert buffer-gas. Frequent collisions between the (optically) active atoms and the buffer-gas atoms effectively suppress the ballistic motion, as illustrated in figure 5(b). Between collisions, the atomic velocity of the active atoms is constant and still governed by the bare thermal distribution. However, the velocity gets redistributed over several collisions (or even upon a single collision in the so-called ‘hard collision’ limit). The overall effect of these frequent velocity-changing collisions is a diffusive motion of the active atoms. For now, we disregard the effect of the collision on the internal state of the atoms, predominantly causing dephasing of the optical transitions (so-called pressure broadening), which we discuss in section 3.4 below.

Given a diffusion coefficient D , the transit time through a typical length scale l is given by l^2/D , resulting in a spectral broadening of

$$\sigma = \frac{D}{l^2}. \quad (34)$$

This should be compared to the broadening due to ballistic motion $\sigma = v_{\text{th}}/l$, and the actual broadening would be the *smaller* of the two. When $D/l^2 < v_{\text{th}}/l$, the diffusion broadening prevails, narrowing the Doppler broadening by the factor $D/(v_{\text{th}}l)$. This effect is known as Dicke narrowing [59, 60]. Note that Dicke narrowing occurs when l (usually the relevant wavelength) is larger than the effective mean free-path between collisions D/v_{th} .

For a single optical transition, the relevant length scale $l = \lambda/(2\pi)$ (on order 100 nm) is typically shorter than the collision mean free-path (a few microns for 10 Torr of buffer gas), and Dicke narrowing is hard to reach (although it has been demonstrated in a nanoscale vapor cell [61]). For most experimental conditions, the motional contribution to the optical line is therefore usually a Gaussian due to Doppler broadening.

On the other hand, the EIT transition has a (two-photon) wavelength $2\pi/|\vec{k}_p \pm \vec{k}_c|$ that, in the case of the Λ level configuration, often surpasses the mean free-path, and hence Dicke narrowing prevails. The EIT line broadening then takes the form of a Lorentzian with a HWHM of $Dk^2 = D(\vec{k}_p - \vec{k}_c)^2$ [62]. For example, in the case of so-called hyperfine EIT, shown in figure 1(a), where the frequency difference $c(\vec{k}_p - \vec{k}_c)$ is on the

order of a few GHz, the two-photon wavelength is a few centimeters. The resulting, Dicke-narrowed, linewidth is a few Hz (for $D \approx 10 \text{ cm}^2 \text{ s}^{-1}$ with 10 Torr buffer gas; see table V in [9] for the diffusion coefficients in common buffer-gasses). This width is much smaller than that expected without a buffer gas ($\sim 10 \text{ kHz}$) and usually negligible compared to other broadening mechanisms.

3.3. Finite beam effects

For a beam of finite width, with a transverse dimension smaller than the extent of the atomic medium, as illustrated in figure 5(c), transverse motion of atoms through the beam results in what is known as transit-time broadening. This spectral broadening can be evaluated according to equation (29) as the inverse of the time of flight through the beam waist

$$\Gamma_{\text{tt}} = \frac{v_{\text{th}}}{w_0} \text{ or } \frac{D}{w_0^2}, \quad (35)$$

where, again, the smaller one prevails.

For a ballistic transverse motion, an exact solution can be obtained by summing susceptibilities for different velocities, similarly to the Doppler broadening due to longitudinal motion (32). However, for transverse motion one must also sum over the different wavevectors of the field interacting with the atoms

$$E_{\text{out}}(\delta) = \int d^2 k_{\perp} E_{\text{in}}(\delta, \vec{k}_{\perp}) e^{ik_{\perp} L} \int d^2 v w(\vec{v}) \chi_{\text{p}}(\delta, k_{\perp}, v), \quad (36)$$

where $E(\delta, \vec{k}_{\perp})$ is the two-dimensional Fourier transform of the transverse envelope of the incoming field. For the general case of EIT, when both the probe and control fields are confined, such a full solution is not trivial. However, it is instructive to consider a more simple case where only the probe field is a finite Gaussian beam. In this case, the solution has a 'cusp'-like lineshape

$$\chi_{\text{ensemble}}(\delta) \propto e^{-|\delta| \frac{w_0}{v_{\text{th}}}}, \quad (37)$$

with a full-width at 1/e of

$$2\Gamma_{\text{tt}} = 2 \frac{v_{\text{th}}}{w_0} \quad (38)$$

or FWHM of $2(v_{\text{th}}/w_0) \log 2$. The cusp shape can be intuitively explained by the nature of the transit time broadening, where slow atoms, which contribute a narrow-line spectrum, also have a larger weight in the overall spectrum due to the longer period of interaction with the probe field. For a vast range of experiments with mm-sized beams, this broadening is on the order of tens of kHz, while for experiments with beams focused to a few microns this already yields a spectral broadening of few MHz, on the order of the natural width of the excited state.

In figure 7, we plot the EIT lineshape for a Λ system under different motional regimes and for realistic finite decoherence rate of the ground states γ_{12} . For a slight angle between the probe and control fields or a slight energy mismatch, such as in the case of hyperfine EIT, the residual Doppler broadening for atoms in ballistic motion results in a Voigt lineshape with reduced contrast (blue dashed line). However, for the same configuration, motion in the diffusive regime can result in a Dicke narrowed line with a width approaching the natural linewidth (solid line). Transit-time broadening due to finite transverse dimensions of the beam results in a cusp lineshape convoluted with the natural Lorentzian lineshape (dashed purple line).

Turning now to discuss the diffusive regime in the transit-time problem, we again differentiate between infinite and finite control fields. In the former case, when only the probe beam is finite, it is enough to (linearly) average over the different wavevector composing the probe field,

$$E_{\text{out}}(\delta) = \int d^2 k_{\perp} E_{\text{in}}(\delta, \vec{k}_{\perp}) e^{ik_{\perp} L} \chi_{\text{p}}(\delta, \vec{k}_{\perp}), \quad (39)$$

where $\chi_{\text{p}}(\delta, \vec{k}_{\perp})$ includes the Dicke-broadened two-photon linewidth $\gamma_{\text{EIT}} + D(k_{\text{p},z} \hat{z} + \vec{k}_{\perp} - \vec{k}_{\text{c}})^2$. For nearly-degenerate, co-propagating probe and control $k_{\text{p},z} \hat{z} \approx \vec{k}_{\text{c}}$, the EIT line is overall broadened by D/w_{p}^2 , where w_{p} is the probe's waist.

As before, the calculation becomes more involved if the control beam is finite as well. For a weak control field, a direct convolution over the control's wavevectors can be done. However for strong control fields, when the power broadening $\Omega_{\text{c}}^2/\sigma_{\text{Dop}}$ is much larger than γ_{12} , the (nonlinear) contribution of the control complicates the calculations. For some arrangements, though, one can perform the calculation in the spatial (rather than the spectral) regime. One notable example is the arrangement of identical probe and control

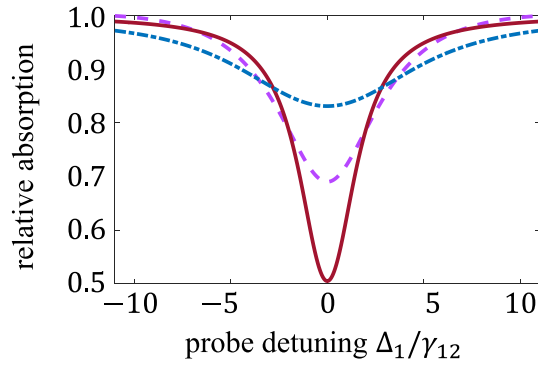


Figure 7. EIT lineshape for various regimes of motional broadening. calculated EIT lineshape with no wavelength mismatch (solid red line), with small wavelength mismatch of 10^{-5} of the optical wavelength (dashed blue line) resulting in a residual Doppler broadening, and with a finite beam width (dashed purple line) resulting in transit-time broadening. In all cases $\gamma_{13} = 3$ MHz, $\gamma_{12} = 1$ kHz, and $\Omega_c = 0.5$ MHz.

fields ($w_p = w_c$), with atoms constantly diffusing in and out of the illuminated area. In this regime, the illuminated periods, interrupted by dark periods, can be thought of as a stochastic train of Ramsey spectroscopy sequences. The resulting EIT line has a characteristic sharp peak (cusp or cusp-like shape) with a typical width γ_{12} , i.e., it is unaffected by power broadening [56, 63]. This effect, known as Ramsey-narrowing, can be explained by the atoms spending a long time outside the beams, in the dark, before the repeated interaction with the optical fields.

Beyond broadening and narrowing, there are several interesting spatial effects occurring in the finite-probe regime. Traversing the medium as a slow-light polariton, the probe field is directly affected by the motion of the atoms. Particularly on EIT resonance, the atoms effectively carry the field with them. As a result, a uniform drift velocity of the atoms results in transverse drag of the probe field [64], while a diffusive motion of the atoms results in spatial diffusion of the field [65–67]. Notably, the diffusion here is of a complex quantity (a ‘coherent diffusion’ of both the argument and the phase of the field) and it therefore demonstrates interference phenomena, such as self-similar expansion and contraction of the probe field [68–70]. More intriguing results occur slightly off the EIT resonance, such as negative drag and negative diffraction [71, 72].

Finally, some atoms reach the enclosing walls of the cell. If the walls are not coated by a spin-preserving material (see section 5 below), the atoms eventually bounce from them completely decohered. They therefore cause a transit-time broadening, which can be described as outlined above for a finite beam, with the cell width replacing w_0 . If the walls are coated, they can manifest, in the ideal case, as a periodic boundary condition. In this case, for degenerate and collinear probe and control fields ($\vec{k}_p \pm \vec{k}_c = 0$) and assuming the beams cover the entire (finite) cell, the situation is akin to an infinite-beam arrangement, and we expect no motional decoherence. More generally, when $\vec{k}_p \pm \vec{k}_c \neq 0$, the cell must be smaller than the two-photon wavelength $2\pi/|\vec{k}_p \pm \vec{k}_c|$ for motional decoherence to be neglected.

3.4. Collisional effects

Up to here, we have discussed the effect of collisions on the atomic motion and the resulting spectral and spatial behaviour. We now turn to consider the effect of the collisions on the atomic internal state. As illustrated in figure 5(d), we consider collisions of active atoms among themselves and collisions with buffer-gas atoms. The latter predominantly decohere the orbital transitions, leading to so-called pressure broadening γ_{13}^{col} of the optical line [73]. This broadening is typically on the order of $\gamma_{13}^{\text{col}} = 10$ MHz per Torr of a buffer gas [74]. The cross-section for relaxation and shift of the spin transition (within the ground level) due to buffer-gas collisions is much smaller, and it becomes important, for example, in miniature atomic clocks [75]. Notably, for ladder EIT which relies on the coherence between electronic orbitals, pressure broadening is always destructive.

On the other hand, collisions amongst the active atoms can introduce substantial spin decoherence γ_{12}^{col} , thus broadening the EIT line in Λ systems. There is collisional cross-section for ‘spin exchange’, which conserves the total spin of the colliding pair [76, 77], and a cross-section for ‘spin destruction’, which relaxes the total spin. The former is usually larger and can reach the kHz regime. The rate of both processes depends on the collision rate, which is linear in the atomic density. This leads to a trade-off when determining the density, as discussed in the next section, with higher densities providing for stronger EIT at the expense of faster collisional relaxation and broader lines.

The spectral broadenings due to collisions γ_{13}^{col} and γ_{12}^{col} are typically considered to be homogeneous, adding to the natural homogeneous linewidths γ_{13} and γ_{12} . For a Λ -type EIT, in the limit $\gamma_{13} + \gamma_{13}^{\text{col}} \gg \sigma_{\text{Dop}}$ (i.e. when the inhomogeneous Doppler broadening of the optical line is relatively small), the EIT linewidth obtains the simple form

$$\gamma_{\text{EIT}} = \frac{\Omega_c^2}{\gamma_{13} + \gamma_{13}^{\text{col}} + \sigma_{\text{Dop}}} + \gamma_{12} + \gamma_{12}^{\text{col}}. \quad (40)$$

Equation (40) also provides a crude approximation when $\gamma_{13} + \gamma_{13}^{\text{col}}$ and σ_{Dop} are comparable; For a more exact result, a calculation including an integration over thermal velocity groups is required. In the general case the calculations typically require numerical calculations of the Voigt integral; however, by approximating the Maxwell velocity distribution with a Lorentzian lineshape, one can obtain a more precise analytical approximation to the EIT linewidth for the case of an arbitrary ratio between homogeneous and inhomogeneous broadenings of the optical transitions [32].

4. How to design the ‘right’ EIT realization in hot vapor

4.1. Important parameters

Different figures of merit of the EIT process may be relevant for different applications. Nevertheless, there are three parameters measurable directly from the EIT absorption spectrum, as illustrated in figure 8(a), that together govern most EIT applications. The first parameter is the resonant optical depth of the medium in the absence of control field. In terms of the absorption coefficient α_0 , the optical depth is defined by $\text{OD} = 2\alpha_0 L$, where L is the medium’s length. The other two parameters are: OD_{EIT} , the reduction in the optical depth at the EIT resonance (defining the relative height of the transmission line); and $2\gamma_{\text{EIT}}$, the full width of the EIT transmission line. To the leading order, these parameters determine the transmission bandwidth, the slow-light (group) delay, and the sensing response, as well as many other important properties.

The transmission on the EIT resonance is given by $e^{-\text{OD} + \text{OD}_{\text{EIT}}}$. High transmission therefore requires that OD_{EIT} approaches OD, which is often referred to as high-contrast EIT. The frequency range around the resonance for which the transmission is still relatively high (e.g. higher than e^{-1} of the maximal transmission $e^{-\text{OD} + \text{OD}_{\text{EIT}}}$) is denoted as the bandwidth B . The bandwidth determines, for example, how short the (slow-light) probe pulse can be before suffering from significantly increased absorption and distortion. Notably, γ_{EIT} is the half-width of the EIT line after taking the logarithm of the absorption spectrum, and it is equal to B only for small OD_{EIT} , see illustration in figure 8(b). As OD_{EIT} increases, the bandwidth decreases, and it is given by $B = \gamma_{\text{EIT}} / \sqrt{\text{OD}_{\text{EIT}} - 1}$, sometimes referred to as the EIT density narrowing [78]. Another aspect is the delay of slow light in the medium, which is given by $\tau = \text{OD}_{\text{EIT}} / \gamma_{\text{EIT}}$. It follows that the time-bandwidth product, which indicates how many separated probe pulses can fit inside the medium, is given by $B\tau \approx \sqrt{\text{OD}_{\text{EIT}}}$ for $\text{OD}_{\text{EIT}} \gg 1$.

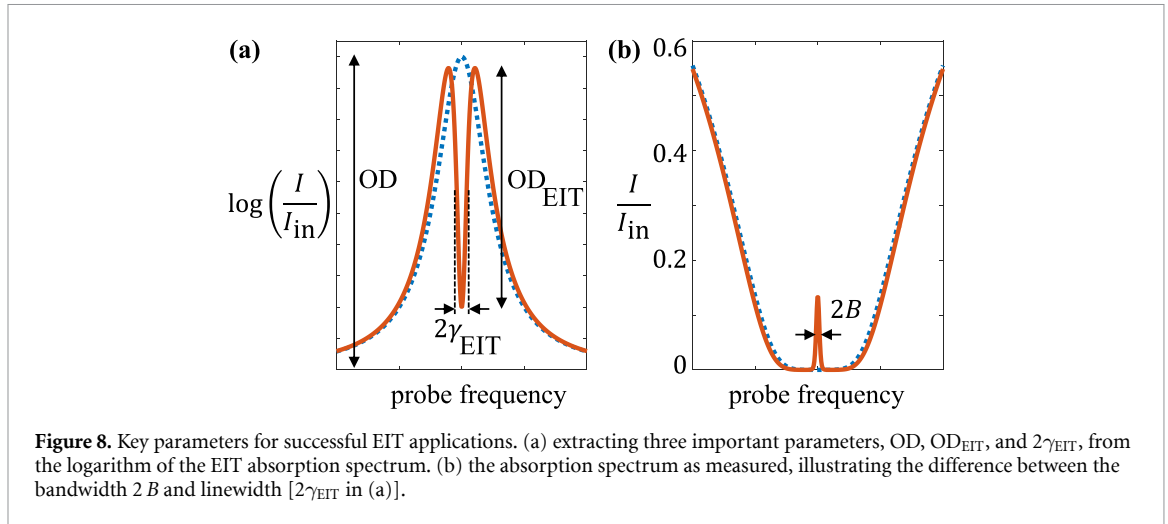
More generally, OD determines the maximal strength of the cooperative light–matter interaction, while OD_{EIT} determines the effective fraction of the OD that is available for controllably coupling light to the ρ_{12} coherence. Therefore, high-fidelity protocols based on EIT require high OD and $\text{OD}_{\text{EIT}} \approx \text{OD}$. For example, the inefficiency of light storage, for probe pulses within the bandwidth B , scales as $1/\text{OD}_{\text{EIT}}$ [14].

To maximize OD and OD_{EIT} while minimizing γ_{EIT} , one desires an optically thick medium with slow spin decoherence processes and a strong control field. This desire encounters many practical trade-offs, which we detail in the next section.

4.2. Trade-offs

An ideal implementation of EIT requires simultaneously using all ideal resources: the highest OD possible, the strongest control Rabi frequency, and the longest coherence time. For example, for high bandwidth operation, one needs a strong Rabi frequency, balanced by the corresponding high OD, to maintain high contrast and low group velocity. However, in real life, all of these resources are limited and can often come at the expense of one another. Designing the experiment is thus the art of striking the balance between different requirements in a way that best serves the goal of a specific experiment. In the following, we list some common trade-offs and note the tensions that may rise when trying to optimize experimental configurations. This is far from being an exhaustive list, and is meant to provide some general guidance while navigating this many-parameter space.

Most EIT experiments use narrowband lasers—either diode or solid-state lasers—with output power usually limited to a few Watt. To account for the limited power and maintain high Rabi frequency, a typical solution is to focus the control field down to increase the local intensity. This, however, limits the size of the probe field which must be contained within the control field. These finite fields deviate from the ideal,



plane-wave description laid out in section 2 and result in both transit-time broadening and inhomogeneity of the control Rabi frequency in the transverse dimension.

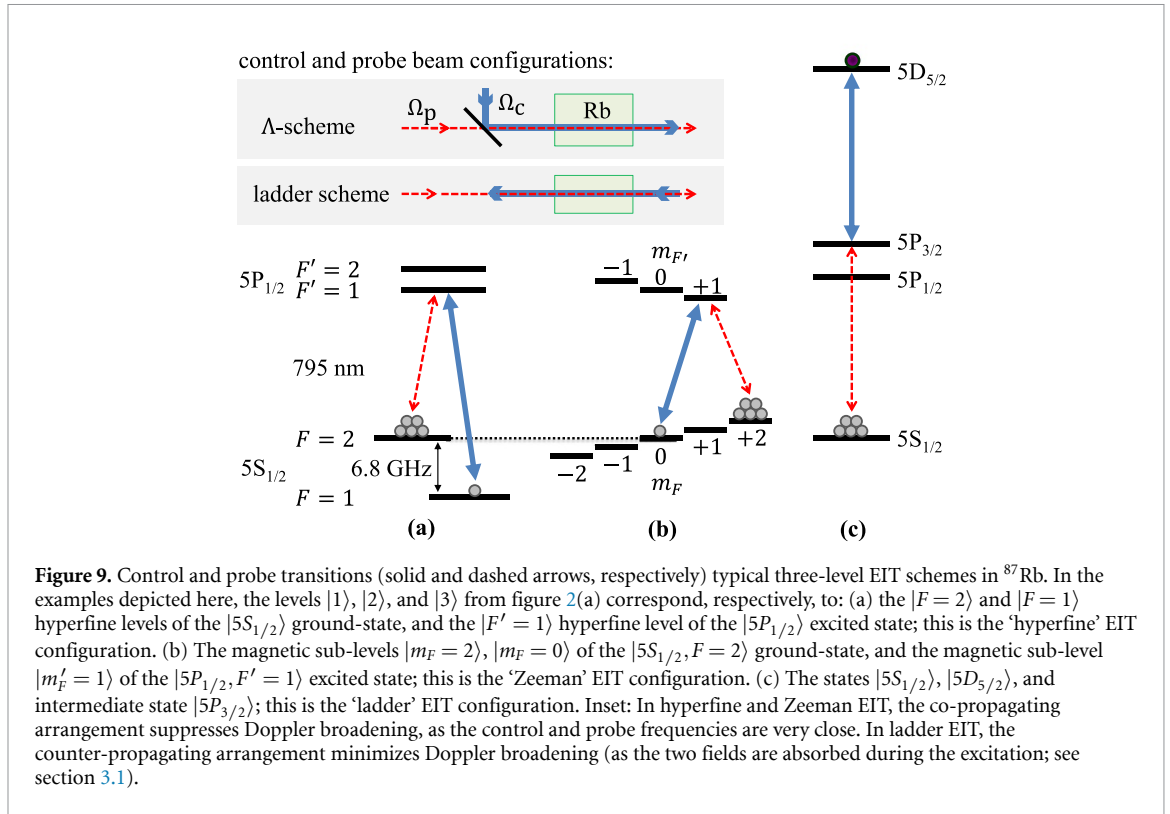
To increase the OD, one can increase the temperature of the vapor cell and by that the atomic density. However, this would also increase the collision rate that may reduce spin lifetime and limit the efficiency of optical pumping. This trade-off can be partially relaxed by using spin transitions that are free of spin-exchange relaxation [79, 80], but spin destruction is always present. In addition, increasing OD results in the enhancement of non-linear light-matter interactions, such as four-wave mixing [81, 82]. Another route to increasing the OD is to elongate the cell, which can result in a non-compact geometry and, more fundamentally, limits the size of the probe and control fields as paraxial diffraction becomes important.

To prolong the spin coherence lifetime, one can increase buffer-gas pressure and thus slow down diffusion to eliminate motional decoherence. However, this increases pressure broadening and would ultimately introduce spin relaxation via collisions. Plus, since collisional dephasing has a much stronger effect on the excited electronic states, this strategy is not possible in ladder EIT. One can decide to work with wall-coating instead of a buffer-gas, in order to reduce spin relaxation at the walls, however current coatings are temperature limited to about 50 °C–100 °C, which limits the atomic density. In case of non-degenerate three-level system, the length of a coated cell must be smaller than the two-photon transition wavelength to avoid spin-wave phase variation across the cell.

5. How to build basic experimental setups

A simple three-level atom as described in section 2 does not really exist. Nevertheless, the three-level model often well captures the interaction in real atoms, such as in Alkali metals. These atoms offer two-photon ground-state transitions that are accessible with relatively low optical power. The ready availability of inexpensive robust laser diodes at wavelengths corresponding to the D lines in Rb and Cs make these particular alkalis especially favored [83]. The most widely used three-level EIT schemes with alkali atoms correspond to the three configurations depicted in figure 1. Examples for the implementation of a hyperfine Λ scheme, Zeeman Λ scheme, and a ladder scheme are illustrated for ^{87}Rb in figures 9(a)–(c). Ladder EIT has recently received increased attention in the context of the use of Rydberg atoms for quantum information experiments [84, 85]; With a two-photon excitation, the level $|2\rangle$ of the three-level model can be either a nS or a nD Rydberg state.

A stable, relative phase between the control and probe fields is required to create the long-lived ground state coherence needed for a robust dark state. Zeeman EIT is the least resource-intensive of the three schemes above, requiring only acousto-optic modulation of the output from a single laser at a few tens of kHz to generate the control and probe frequencies resonant with the Zeeman-shifted sub-levels, as depicted in figure 9(b). Hyperfine EIT requires two phase-locked lasers each tuned to the hyperfine optical transitions, as depicted in figure 9(a) [86, 87]. Alternatively, one can use various modulation techniques to derive both fields from the same laser. The choice of modulation technique depends on the application, and on the alkali metal used. If the modulation frequency is smaller than ≈ 3.5 GHz, one can generate a probe field by double-passing a high-frequency acousto-optical modulator (AOM) [88]; this approach works well for alkali metals with smaller ground-state hyperfine splitting values, such as Na and ^{85}Rb [89, 90]. The advantage of such an approach is that the generated probe field is a physically separate beam, and its optical properties can

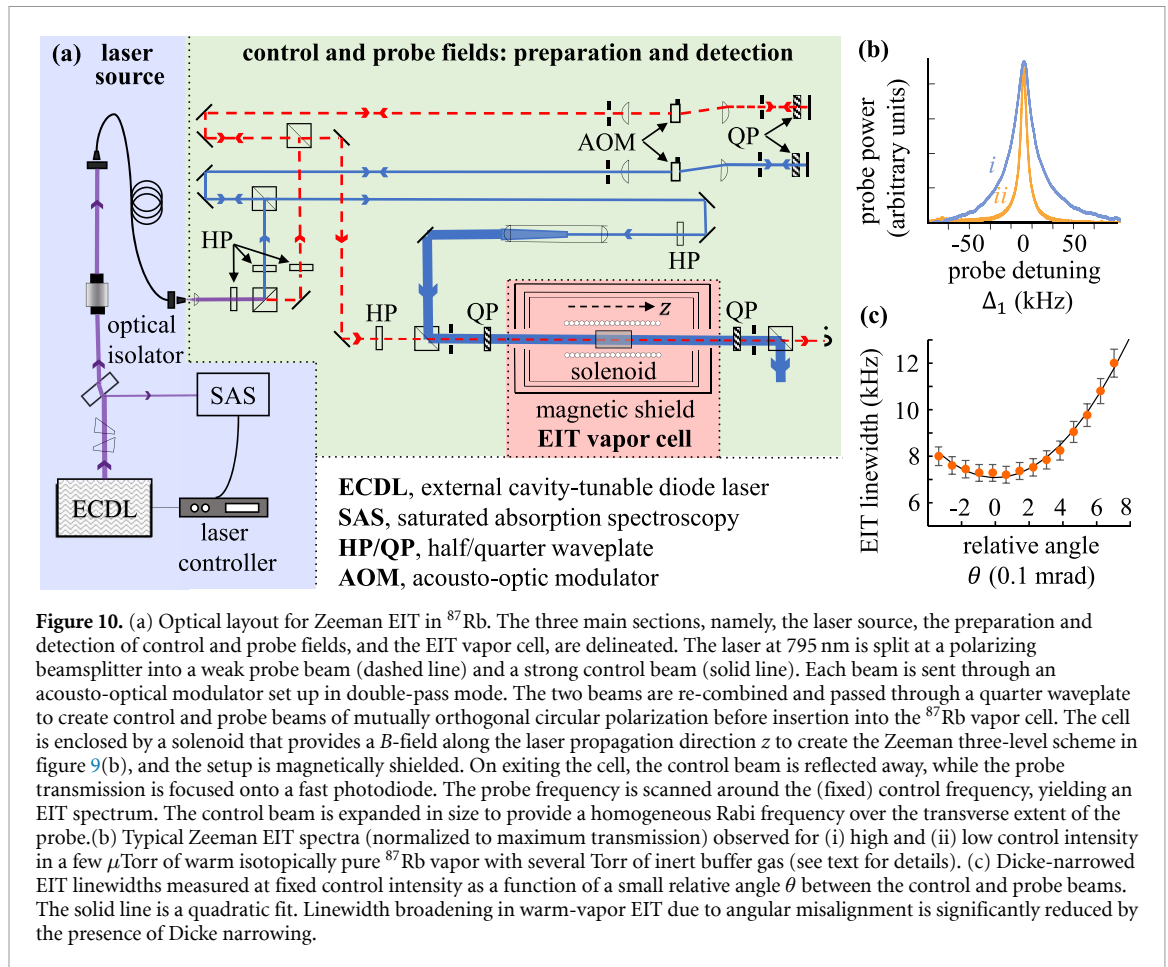


be manipulated independently of the control field. The drawback is the low efficiency of AOMs at such high frequency. If higher modulation frequency is required, electro-optical modulators (EOMs) are the best choice [91, 92]; modern fiber EOMs are broadband and can achieve high modulation efficiency even at moderate rf power. The drawback of this method is that the carrier and all modulation sidebands emerge perfectly spatially overlapped, so that either the experiment must operate with the control and probe fields in the same spatial mode and polarization, or additional filtering must be employed to separate the desired modulation sideband. Moreover, potential complications may arise due to coupling of the off-resonant modulation sideband into the atomic system, for example leading to undesirable multi-wave mixing processes [81]. Also, while most of the diode lasers do not allow direct current modulation above 1 GHz, vertical cavity surface emitting lasers (VCSELs) have very fast response time and can be modulated at frequencies up to tens of GHz [93]. This modulation method is particularly attractive for development of chip-scale atomic clocks (CSAC) and magnetometers [4, 94–96]. However, the low output power and broad linewidth of VCSELs limits their applicability for most other situations. Finally, ladder-EIT schemes, especially those involving Rydberg atoms, use control and probe lasers that are much farther apart in frequency, by up to hundreds of nanometers; in this case the frequency lock is often used to keep the lasers on the two-photon resonance [97].

An optical layout showing some general features of an EIT setup, in the specific context of Zeeman EIT in ^{87}Rb , is depicted in figure 10(a) and briefly discussed below. For further experimental details, please refer to [46].

5.1. Laser source

For many alkali-based EIT experiments, it suffices to use lasers that provide low power (20–40 mW), have a linewidth much narrower than the Doppler linewidth in warm vapor ($\ll 100$ MHz), and are frequency-tunable over the ground state hyperfine splitting (2–10 GHz, depending on choice of alkali). Grating-feedback-tuned external cavity diode lasers (ECDL) with a typical laser linewidth of a few hundred kHz, or distributed feedback diode lasers with linewidth of 1–2 MHz, satisfy all these parameters and are commercially available; these lasers are widely used in EIT experiments. One of the known problems of the diode laser is asymmetry and astigmatism of the output beam. To solve this problem, typically the output of a diode laser is coupled into a single-mode polarization maintaining optical fiber, as shown in figure 10(a). The main purpose of the fiber is to create a clean Gaussian output beam profile with polarization drift of no more than a few percent. An optical isolator, placed in between, suppresses frequency-destabilizing back-reflection from the fiber into the laser. If the output beam out of a diode laser is strongly anisotropic, an anamorphic prism pair can be used to circularize its elliptical cross-section and improve coupling efficiency



into the fiber. Figure 10(a) also shows that a small portion of the EC DL output is split off with a glass window to stabilize the laser frequency near the $F = 2 \rightarrow F' = 1$ D1 transition (see figure 9(b)) using, for example, the method of saturated absorption spectroscopy [83].

Solid state laser systems, such as stabilized continuous-wave Ti:Sapph lasers [98] are the best for an experiment requiring higher laser power, as they can output up to several watt of narrow-band optical field, tunable in a very wide spectral range. These laser systems also provide a much cleaner output spatial mode and do not have a broad-spectral background emission that is typical of diode lasers. However, they are significantly more expensive.

5.2. Control and probe field preparation and detection

The output from the fiber is split into two orthogonally linearly polarized beams with a polarizing beamsplitter (PBS) to create a weak probe beam (dashed line) and a strong control beam (solid line). Each beam is fed into an AOM to enable tuning of the control and probe frequencies so as to satisfy the two-photon resonance condition. The AOMs also enable the scanning of the probe frequency around the fixed control frequency, where the double-pass AOM configuration suppresses spatial misalignment of the beam during the scanning. To avoid slow frequency and phase drifts between the control and probe fields, the AOMs are driven by twin phase-locked rf signals from the same dual-output waveform generator.

As described in sections 2 and 3, the linewidth of the EIT resonance γ_{EIT} depends upon the control field intensity, which should therefore be ideally uniform in the region of spatial overlap with the probe. One method to approximately satisfy this is to expand the control beam to a size significantly larger than the probe, prior to recombining the two beams and inserting into the vapor cell. Expanding the control beam also allows us to use a larger probe beam, which helps combat transit-time broadening in vapor cells without buffer gas or wall coatings, as indicated previously in section 4.2.

For Zeeman EIT, the control and probe beams must have mutually orthogonal circular polarization, which is achieved by placing a quarter waveplate (QP) in the path immediately before the cell. Upon exiting the cell, a second QP converts the circular polarizations back into linear, which enables separation of the probe and control beams at a PBS. The weak probe transmits through and is focused onto a photodiode, while the strong control beam is reflected away. It is important to minimize leakage of the strong control

beam into the photodiode; a Glan–Taylor prism with an extinction ratio of 10^5 may be employed for the probe–control beam separation [all other PBS in figure 10(a) provide a typical extinction of 10^3].

5.3. EIT vapor cell

A typical atomic vapor cell is a pyrex cylinder (or sometimes a cube), with a stem (side arm) containing a few mg of solid Rb or Cs. If the cell has bare polished glass windows, one must expect approximately 20% losses due to reflection of the windows. Moreover, the reflected beams may perturb the atomic coherence and distort the EIT signal [99]. Luckily, vapor cells with anti-reflection coatings on both sides of the quartz windows are now available.

The content of an experimental cell also depends on the details of the applications. One ingredient—alkali metal—is necessary, of course. The choice of specific element is sometimes determined by its properties, such as the number of Zeeman sublevels or the separation between excited state levels, but often is driven by the available equipment and previous work of the research group. Also, for alkali metals having more than one isotope, it is important to decide if natural abundance mixture of isotopes is sufficient, or isotopically enriched metal must be used (at an additional cost).

The next step is to choose any additions to the pure metal, especially for the experiments with Λ -type interactions. As discussed in section 3.2, in many experiments a few Torr of inert ‘buffer’ gas, such as He, Ne, or N_2 , are introduced to extend the confinement time of alkali atoms within the illuminated volume by orders of magnitude [100]. Another possible approach is to coat the cell walls with a derivative of paraffin (tetracontane $C_{40}H_{82}$ seems to be the top choice), to help preserve spin coherence during atom-wall collisions. Paraffin coatings break down at higher temperatures (typically 60°C – 80°C) [101]. If high atomic density is required, one may opt for OTS (octadecyltrichlorosilane) coatings which withstand higher temperatures [102], although the spin-preserving characteristics of OTS seem to be inferior compared to paraffin. Also, since very few commercial sources for wall-coated cells exist, it may not be trivial to procure an antirelaxation coating cell, causing some users to just develop their own in-house coating capabilities.

To control the density of atoms in the experiment, the stem containing the metal can be slightly heated, changing the saturated pressure of alkali vapor, typically on the order of a few μTorr , corresponding to an atom number density of 10^{11} – 10^{12} cm^{-3} [103]. It is important to heat the cell uniformly and use a bifilar heating wire or other heating methods which do not inject undesired magnetic fields into the sample. The heating wire may be wrapped around the innermost magnetic shield layer (see below) to allow air to circulate for uniform heating.

The optimal operational temperature is typically determined by optimizing the experimental performance. On one hand, as indicated in section 4.1, the EIT linewidth γ_{EIT} is modified by the optical depth of the sample to yield a useful ‘effective EIT bandwidth’ given by $B \sim \gamma_{\text{EIT}}/\sqrt{\text{OD}_{\text{EIT}}}$ (see figure 8). Raising the atom density raises the optical depth and narrows the bandwidth B . Moreover, equations (15) and (28) explicitly show that the group velocity v_g is lowered at higher atom density N . Clearly, keeping the number density N high is desirable for many EIT-based quantum applications. On the other hand, raising N too much may actually deteriorate EIT performance, by, e.g. increasing undesirable spin-relaxation collisions (see section 4.2) and introducing additional density-dependent relaxation mechanisms. For example, radiation trapping—the reabsorption of spontaneously emitted photons within the illuminated volume—reduces the average spin coherence lifetime. It becomes significant at densities $\geq 5 \times 10^{11}$ cm^{-3} for the typical mm-sized laser beam diameters that are employed in vapor cell experiments [104].

Another important decoherence mechanism that contributes to the ground-state decoherence rate is residual magnetic field inhomogeneity [31, 46]. In the case of Zeeman EIT, for example, this causes spatial variation of the dark state leading to dephasing. As indicated in figure 10(a), the cell is placed inside a solenoid which provides controlled dc magnetic fields along the laser propagation direction. The solenoid can be used either for near-complete cancellation of residual fields, so that the Zeeman sub-levels stay degenerate, or for adding a well-defined magnetic field (typically 10–100 mG) that separates the Zeeman sub-levels. This separation is advantageous for both Zeeman and hyperfine EIT when only one desired transition (e.g. the clock transition $m_F = 0$) is to be addressed. The vapor cell and solenoid are enclosed by a triple-layer of high-magnetic permeability alloy which shields the cell from unwanted external magnetic fields. Before taking any data, the shield must be demagnetized by a degaussing technique using coils wound around one or more of the shielding layers [46].

5.4. Probe transmission spectra

To generate an EIT spectrum, the two-photon detuning is adjusted by varying the relative detuning between the probe and control frequencies, and the probe transmission is recorded. This is achieved by scanning the probe AOM around the control frequency which is held fixed. In the Zeeman EIT scheme depicted in figure 9(b), the Zeeman shifts between the magnetic sub-levels of the $F = 2$ ground state are 0.7 kHz mG^{-1} ,

so a B_z field of 50 mG from the solenoid splits adjacent ground sub-states 35 kHz apart, and a probe scan of less than ± 100 kHz suffices to record the EIT spectral feature. In figure 10(b), Zeeman EIT spectra observed in a few μ Torr of isotopically pure ^{87}Rb vapor with 10 Torr of Ne buffer gas at about 60°C are shown for two different control intensities: (a) 5.5 mW cm^{-2} and (b) 1.3 mW cm^{-2} , corresponding to $\Omega_c/2\pi = 3.9\text{ MHz}$ and 1.9 MHz , respectively. The spectra are displayed on the same vertical scale to enable a visual linewidth comparison. The FWHM, extracted by Lorentzian fits that are normalized to the same amplitude at zero detuning, yield EIT linewidths of 26 kHz and 7.3 kHz respectively. The ratio of almost 4 between the two linewidths, as also between the two control intensities, is indeed what one expects if the EIT lines are dominated by power broadening.

Perfect co-linear alignment of the control and probe beams in EIT is an idealization. In the experiment, a slight angle between the two beams exists, which introduces a residual or two-photon Doppler broadening, as discussed above in section 3.1. For the Λ -scheme with close-lying control and probe frequencies, we may straightforwardly estimate the residual Doppler broadening to be $k_{\text{eff}} \cdot \vec{v} \approx |\vec{k}| v_{\text{th}} \theta = \sigma_{\text{Dop}} \theta$. Thus, even for a slight relative angle $\theta \sim 0.1$ mrad, with typical Doppler broadening of a few hundred MHz in the warm vapor cell, we see that the two-photon Doppler broadening is tens of kHz and is significant in Λ -type EIT. However, in the presence of a buffer gas, frequent velocity-changing collisions prevail, which cause Dicke narrowing of the Doppler broadening as discussed in section 3.2. It is mentioned there that the resulting Dicke-narrowed EIT linewidth follows a quadratic dependence on θ instead of linear; this statement is borne out by the data in figure 10(c). Here, the control and probe beam sizes ($1/e^2$ -radii 2.55 mm and 0.47 mm, respectively) and intensities (1.3 mW cm^{-2} and 0.12 mW cm^{-2} , respectively) are the same as in curve (ii) of figure 10(b). The optical depth is ~ 10 . The solid line is a quadratic fit to the data. The data shows that the EIT linewidth remains narrow despite angular mismatch between the control and probe beams. Thus the tolerance for angular deviation in applications utilizing warm vapor is increased significantly owing to the presence of Dicke narrowing [62].

6. Conclusion and outlook

Atomic vapor cells bear with them the promise of a feasible and scalable quantum technology. In the last two decades EIT and its analogues have been considered for a wide range of applications, some of which have already matured into practical devices. Below we briefly discuss some of the notable ones enabled by EIT in atomic vapor.

6.1. EIT-based metrology tools

Measurements of energy separation between various alkali spin states lie at the heart of many precise atomic clocks and magnetometer [75]. The frequencies of these transitions are in the radio-frequency or microwave spectral range, which hinders the development of compact devices as their size may be limited by the transition wavelength. Since a Λ -system EIT allows all-optical coupling to these transitions, it is particularly attractive for miniaturization purposes [3]. In particular, there has been a lot of progress on the development of the CSAC that use microfabricated vapor cells and now achieve fractional frequency stability down to 10^{-11} [105]. The development of EIT-based magnetometers has attracted less attention [95, 106, 107], although several publications have pointed out some of their unique capabilities, e.g. the ability to determine the direction of the magnetic field [108, 109].

It is more common to see references to CPT-based atomic clocks and magnetometers, since the majority of experiments use a balanced Λ -system with equal or nearly-equal intensities of the two optical fields. This configuration allows reduction of some systematic effects like light shifts and can be realized experimentally via direct frequency modulation of a single laser. VCSELs are often used thanks to their excellent modulation response in the GHz range [93]. The miniaturization requirements also lead to the frequent use of vapor cells with relatively high buffer gas pressures. Occasionally, a mixture of gasses is used to reduce the temperature variation of the collisional shifts and improve clock stability [110]. Also, a dynamic Raman–Ramsey interrogation scheme has been successfully implemented to suppress the power broadening of EIT/CPT resonances [34, 111, 112].

More recently, ladder EIT resonances have found use for electrometry that takes advantage of the extreme sensitivity of the Rydberg atomic state to external electric fields [113]. Due to the long lifetime between an electronic ground state and a Rydberg state it is possible to obtain relatively narrow transmission resonances even in a thermal vapor [35, 36]. Monitoring the transmission of the ‘bottom’ optical field of the ladder (E_1 in figure 1(c)), one can accurately track the energy splitting and shift of the Rydberg level, thus gaining information about external microwave or rf electric field [114–117]. The use of vapor-cell EIT-based Rydberg atomic systems has been also explored as an alternative technology for audio and video receivers [118, 119], spectrum analyzer [120], SI-traceable standards [121], etc.

6.2. Quantum information processing

As we have mentioned in section 2.4, the fact that EIT is intimately linked to the existence of a dark state and permits dynamic control over the group velocity of the DSPs can be utilized to store photonic information. The information could be encoded by a number-state qubit (for example zero excitation or a single excitation in a mode), a polarization qubit, a time-bin qubit, or a spatial dual-rail qubit. Such information can also be encoded in continuous variables, as the quadratures of the electromagnetic field. EIT based memories, both in hot vapor as well as in ultracold atoms, were shown to be tuned to reach very high efficiency, noise-free operation, and large bandwidth [122–124]. Ongoing efforts aim to combine several of these and first commercial applications are already available [125]. The material part of such DSPs can also be realized as a Rydberg excitation. Working at the single-photon level, strongly interacting Rydberg DSPs have been shown to mediate effective photon–photon interactions resulting in phenomena such as single photon trains, photonic molecules, single-photon transistor, and controlled phase gate between photons [84, 126–129].

6.3. EIT as a spectral filter

Narrow EIT resonances can be used to shape the fluctuations of broadband optical probe field, as only the frequencies within the EIT transmission window will emerge after the interaction. The narrow (sub-MHz) tunable EIT linewidth provides a potential alternative to traditional spectral filters based on optical cavities, as both transmissive and dispersive properties of EIT resonance can be adjusted via the control field parameter [130, 131]. In particular, several experiments demonstrated the transmission of squeezed light through EIT [132, 133], as well as squeezed pulse propagation in slow [134, 135], stored [136], and fast light [137] regimes.

If placed inside a cavity, EIT can serve as a control tool for cavity characteristics. For example, it was recognized relatively early in EIT history that intracavity EIT leads to significant cavity linewidth narrowing [138, 139]. More recently, the role of intracavity EIT or similar narrow multiphoton resonances have been considered: For example, a proposal for enhancement of the laser gyroscope performance using superluminal intracavity atomic medium has attracted a lot of attention [49]. At the same time, a subluminal regime was shown to lead to reduced sensitivity to cavity fluctuations and correspondingly a more stable laser operation [140].

The future holds great promise for EIT in atomic vapors. There is a constant development of new paradigms, one recent example we have discussed above is electric field sensors based on EIT with warm Rydberg atoms [117, 141]. Such developments are accompanied by technological maturation of miniature-cell fabrication [26, 142–144], which provides more robust, versatile, and compact platforms for EIT utilization. In parallel to academic research, the technology is also developed in the industry, in both large and small companies. All this progress suggests that we are far from hearing the last word from this diverse field.

Data availability statement

All data that support the findings of this study are included within the article (and any supplementary files).

Acknowledgments

OF acknowledges financial support by the Israel Science Foundation and the Laboratory in Memory of Leon and Blacky Broder. S B acknowledges financial support by the U. S. Army Research Laboratory and the U. S. Army Research Office under Grant Number W911NF2110120. IN acknowledges financial support by the Defense Advanced Research Projects Agency (DARPA) under the US Army Research Office (ARO) Award W911NF-21-2-0094. RF acknowledges support from the Troesh postdoctoral fellowship.

ORCID iDs

Ran Finkelstein  <https://orcid.org/0000-0002-4524-5875>

Ofer Firstenberg  <https://orcid.org/0000-0001-8905-9954>

References

- [1] Harris S E 1997 Electromagnetically induced transparency *Phys. Today* **50** 36
- [2] Fleischhauer M, Imamoglu A and Marangos J P 2005 Electromagnetically induced transparency: optics in coherent media *Rev. Mod. Phys.* **77** 633–73
- [3] Vanier J 2005 Atomic clocks based on coherent population trapping: a review *Appl. Phys. B* **81** 421–42
- [4] Kitching J 2018 Chip-scale atomic devices *Appl. Phys. Rev.* **5** 031302

- [5] Beausoleil R G, Munro W J, Rodrigues D A and Spiller T P 2004 Applications of electromagnetically induced transparency to quantum information processing *J. Mod. Opt.* **51** 2441–8
- [6] Firstenberg O, Adams C S and Hofferberth S 2016 Nonlinear quantum optics mediated by Rydberg interactions *J. Phys. B: At. Mol. Opt. Phys.* **49** 152003
- [7] Lijun M, Slattery O and Tang X 2017 Optical quantum memory based on electromagnetically induced transparency *J. Opt.* **19** 043001
- [8] Wei S-H *et al* 2022 Towards real-world quantum networks: a review (arXiv:2201.04802)
- [9] Happer W 1972 Optical pumping *Rev. Mod. Phys.* **44** 169–249
- [10] Scully M O 1992 From lasers and masers to phaseonium and phasers *Phys. Rep.* **219** 191–201
- [11] Fleischhauer M and Lukin M D 2000 Dark-state polaritons in electromagnetically induced transparency *Phys. Rev. Lett.* **84** 5094–7
- [12] Lukin M D 2003 Colloquium: Trapping and manipulating photon states in atomic ensembles *Rev. Mod. Phys.* **75** 457
- [13] Gorshkov A V, André A, Lukin M D and Sørensen A S 2007 Photon storage in Λ -type optically dense atomic media. II. Free-space model *Phys. Rev. A* **76** 033805
- [14] Gorshkov A V, André A, Fleischhauer M, Sørensen A S and Lukin M D 2007 Universal approach to optimal photon storage in atomic media *Phys. Rev. Lett.* **98** 123601
- [15] Boller K-J, Imamoğlu A and Harris S E 1991 Observation of electromagnetically induced transparency *Phys. Rev. Lett.* **66** 2593–6
- [16] Kocharovskaya O A and Khanin Y I 1986 Population trapping and coherent bleaching of a three-level medium by a periodic train of ultrashort pulses *JETP* **63** 945–50
- [17] Arimondo E and Orriols G 1976 *Nuovo Cimento Lett.* **17** 333
- [18] Arimondo E 1996 Coherent population trapping in laser spectroscopy *Progr. Opt.* **35** 259–354
- [19] Lazoudis A, Kirova T, Ahmed E H, Qi P, Huennekens J and Lyyra A M 2011 Electromagnetically induced transparency in an open v-type molecular system *Phys. Rev. A* **83** 063419
- [20] Lechner R, Maier C, Hempel C, Petar Jurcevic B P, Lanyon T M, Brownnutt M, Blatt R and Roos C F 2016 Electromagnetically-induced-transparency ground-state cooling of long ion strings *Phys. Rev. A* **93** 053401
- [21] Bigelow M S, Lepeshkin N N and Boyd R W 2003 Observation of ultraslow light propagation in a ruby crystal at room temperature *Phys. Rev. Lett.* **90** 113903
- [22] Fulton D J, Shepherd S, Moseley R R, Sinclair B D and Dunn M H 1995 Continuous-wave electromagnetically induced transparency: a comparison of ν , Λ and cascade systems *Phys. Rev. A* **52** 2302–11
- [23] Houmark J, Nielsen T R, Mørk J and Jauho A-P 2009 Comparison of electromagnetically induced transparency schemes in semiconductor quantum dot structures: Impact of many-body interactions *Phys. Rev. B* **79** 115420
- [24] Zektzer R, Talker E, Barash Y, Mazurski N, Stern L and Levy U 2021 Atom-photon interactions in atomic cladded waveguides: Bridging atomic and telecom technologies *ACS Photon.* **8** 879–86
- [25] Thaicharoen N, Moore K R, Anderson D A, Powel R C, Peterson E and Raithe G 2019 Electromagnetically induced transparency, absorption and microwave-field sensing in a Rb vapor cell with a three-color all-infrared laser system *Phys. Rev. A* **100** 063427
- [26] Simons M T, Gordon J A and Holloway C L 2018 Fiber-coupled vapor cell for a portable Rydberg atom-based radio frequency electric field sensor *Appl. Opt.* **57** 6456–60
- [27] Kuang L-M, Chen G-H and Yong-Shi W 2003 Nonlinear optical properties of an electromagnetically induced transparency medium interacting with two quantized fields *J. Opt. B: Quantum Semiclass. Opt.* **5** 341–8
- [28] Sautenkov V A, Li H, Rostovtsev Y V, Welch G R, Davis J P, Narducci F A and Scully M O 2009 Using phase dynamics in EIT to probe ground state relaxation in rubidium vapor *J. Mod. Opt.* **56** 975–9
- [29] Walmsley I A 2015 Quantum optics: Science and technology in a new light *Science* **348** 525–30
- [30] Scully M O and Zubairy M S 1997 *Quantum Optics* (Cambridge: Cambridge University Press)
- [31] Xiao Y 2009 Spectral line narrowing in electromagnetically induced transparency *Mod. Phys. Lett. B* **23** 661–80
- [32] Lee H, Rostovtsev Y, Bednar C J and Javan A 2003 From laser induced line narrowing to electromagnetically induced transparency: closed system analysis *Appl. Phys. B* **76** 33–39
- [33] Mikhailov E E, Novikova I, Rostovtsev Y V and Welch G R 2004 Buffer-gas induced absorption resonances in Rb vapor *Phys. Rev. A* **70** 033806
- [34] Zanon-Willette T, Emeric de C and Arimondo E 2011 Ultrahigh-resolution spectroscopy with atomic or molecular dark resonances: exact steady-state line shapes and asymptotic profiles in the adiabatic pulsed regime *Phys. Rev. A* **84** 062502
- [35] Mohapatra A K, Jackson T R and Adams C S 2007 Coherent optical detection of highly excited Rydberg states using electromagnetically induced transparency *Phys. Rev. Lett.* **98** 113003
- [36] Kübler H, Shaffer J P, Baluksian T, Löw R and Pfau T 2010 Coherent excitation of Rydberg atoms in micrometre-sized atomic vapour cells *Nat. Photon.* **4** 112–16
- [37] Anisimov P M, Dowling J P and Sanders B C 2011 Objectively discerning Autler-Townes splitting from electromagnetically induced transparency *Phys. Rev. Lett.* **107** 163604
- [38] Giner L *et al* 2013 Experimental investigation of the transition between Autler-Townes splitting and electromagnetically-induced-transparency models *Phys. Rev. A* **87** 013823
- [39] Zibrov A S, Lukin M D, Hollberg L, Nikonov D E, Scully M O, Robinson H G and Velichansky V L 1996 Experimental demonstration of enhanced index of refraction via quantum coherence in Rb *Phys. Rev. Lett.* **76** 3935–8
- [40] Yavuz D D 2005 Refractive index enhancement in a far-off resonant atomic system *Phys. Rev. Lett.* **95** 223601
- [41] Hau L V, Harris S E, Dutton Z and Behroozi C H 1999 Light speed reduction to 17 metres per second in an ultracold atomic gas *Nature* **397** 594–8
- [42] Kash M M, Sautenkov V A, Zibrov A S, Hollberg L, Welch G R, Lukin M D, Rostovtsev Y, Fry E S and Scully M O 1999 Ultraslow group velocity and enhanced nonlinear optical effects in a coherently driven hot atomic gas *Phys. Rev. Lett.* **82** 5229–32
- [43] Budker D, Kimball D F, Rochester S M and Yashchuk V V 1999 Nonlinear magneto-optics and reduced group velocity of light in atomic vapor with slow ground state relaxation *Phys. Rev. Lett.* **83** 1767–70
- [44] Milonni P W 2005 *Fast Light, Slow Light and Left-Handed Light* 1st edn (London: IOP Publishing Ltd)
- [45] Novikova I, Walsworth R L and Xiao Y 2012 Electromagnetically induced transparency-based slow and stored light in warm atoms *Laser Photon. Rev.* **6** 333–53
- [46] DeRose K, Jiang K, Jianqiao Li, Zhuo L, Cai H and Bali S 2020 Producing slow light in warm alkali vapor using electromagnetically induced transparency *Am. J. Phys.* **91** 193–205
- [47] Mikhailov E E, Sautenkov V A, Novikova I and Welch G R 2004 Large negative and positive delay of optical pulses in coherently prepared dense Rb vapor with buffer gas *Phys. Rev. A* **69** 063808

- [48] Wang L J, Kuzmich A and Dogariu A 2000 Gain-assisted superluminal light propagation *Nature* **406** 277–9
- [49] Shahriar M S, Pati G S, Tripathi R, Gopal V, Messall M and Salit K 2007 Ultrahigh enhancement in absolute and relative rotation sensing using fast and slow light *Phys. Rev. A* **75** 053807
- [50] Liu C, Dutton Z, Behroozi C H and Hau L V 2001 Observation of coherent optical information storage in an atomic medium using halted light pulses *Nature* **409** 490–3
- [51] Phillips D F, Fleischhauer A, Mair A, Walsworth R L and Lukin M D 2001 Storage of light in atomic vapor *Phys. Rev. Lett.* **86** 783–6
- [52] Zibrov A S, Matsko A B, Kocharovskaya O, Rostovtsev Y V, Welch G R and Scully M O 2002 Transporting and time reversing light via atomic coherence *Phys. Rev. Lett.* **88** 103601
- [53] Simon C et al 2010 Quantum memories *Eur. Phys. J. D* **58** 1–22
- [54] Khabat Heshami D G, England P C, Humphreys P J, Bustard V M, Acosta J N and Sussman B J 2016 Quantum memories: emerging applications and recent advances *J. Mod. Opt.* **63** 2005–28
- [55] Duan L-M, Lukin M D, Cirac J I and Zoller P 2001 Long-distance quantum communication with atomic ensembles and linear optics *Nature* **414** 413
- [56] Firstenberg O, Shuker M, Pugatch R, Fredkin D R, Davidson N and Ron A 2008 Theory of thermal motion in electromagnetically induced transparency: Effects of diffusion, doppler broadening and Dicke and Ramsey narrowing *Phys. Rev. A* **77** 043830
- [57] Finkelstein R, Lahad O, Michel O, Davidson O, Poem E and Firstenberg O 2019 Power narrowing: counteracting Doppler broadening in two-color transitions *New J. Phys.* **21** 103024
- [58] Finkelstein R, Lahad O, Cohen I, Davidson O, Kiriati S, Poem E and Firstenberg O 2021 Continuous protection of a collective state from inhomogeneous dephasing *Phys. Rev. X* **11** 011008
- [59] Dicke R H 1953 The effect of collisions upon the doppler width of spectral lines *Phys. Rev.* **89** 472–3
- [60] Firstenberg O, Shuker M, Ben-Kish A, Fredkin D R, Davidson N and Ron A 2007 Theory of Dicke narrowing in coherent population trapping *Phys. Rev. A* **76** 013818
- [61] Sargsyan A, Pashayan-Leroy Y, Leroy C and Sarkisyan D 2016 Collapse and revival of a Dicke-type coherent narrowing in potassium vapor confined in a nanometric thin cell *J. Phys. B: At. Mol. Opt. Phys.* **49** 075001
- [62] Shuker M, Firstenberg O, Pugatch R, Ben-Kish A, Ron A and Davidson N 2007 Angular dependence of Dicke-narrowed electromagnetically induced transparency resonances *Phys. Rev. A* **76** 023813
- [63] Xiao Y, Novikova I, Phillips D F and Walsworth R L 2006 Diffusion-induced Ramsey narrowing *Phys. Rev. Lett.* **96** 043601
- [64] Solomons Y, Banerjee C, Smartsev S, Friedman J, Eger D, Firstenberg O and Davidson N 2020 Transverse drag of slow light in moving atomic vapor *Opt. Lett.* **45** 3431–4
- [65] Shuker M, Firstenberg O, Pugatch R, Ron A and Davidson N 2008 Storing images in warm atomic vapor *Phys. Rev. Lett.* **100** 223601
- [66] Firstenberg O, Shuker M, Ron A and Davidson N 2013 Colloquium: Coherent diffusion of polaritons in atomic media *Rev. Mod. Phys.* **85** 941
- [67] Chriki R, Smartsev S, Eger D, Firstenberg O and Davidson N 2019 Coherent diffusion of partial spatial coherence *Optica* **6** 1406–11
- [68] Pugatch R, Shuker M, Firstenberg O, Ron A and Davidson N 2007 Topological stability of stored optical vortices *Phys. Rev. Lett.* **98** 203601
- [69] Firstenberg O, London P, Yankelev D, Pugatch R, Shuker M and Davidson N 2010 Self-similar modes of coherent diffusion *Phys. Rev. Lett.* **105** 183602
- [70] Smartsev S, Chriki R, Eger D, Firstenberg O and Davidson N 2020 Structured beams invariant to coherent diffusion *Opt. Express* **28** 33708–17
- [71] Firstenberg O, London P, Shuker M, Ron A and Davidson N 2009 Elimination, reversal and directional bias of optical diffraction *Nat. Phys.* **5** 665–8
- [72] Banerjee C, Solomons Y, Nicholas Black A, Marcucci G, Eger D, Davidson N, Firstenberg O and Boyd R W 2021 Anomalous optical drag (arXiv:2109.02534)
- [73] Allard N and Kielkopf J 1982 The effect of neutral nonresonant collisions on atomic spectral lines *Rev. Mod. Phys.* **54** 1103–82
- [74] Pitz G, Wertepny D and Perram G 2009 Pressure broadening and shift of the cesium d1 transition by the noble gases and N₂, H₂, HD, D₂, CH₄, C₂H₆, CF₄ and 3He *Phys. Rev. A* **80** 12
- [75] Vanier J and Audoin C 1989 *The Quantum Physics of Atomic Frequency Standards* vol 1 (Philadelphia: Adam Hilger)
- [76] Happer W and Tang H 1973 Spin-exchange shift and narrowing of magnetic resonance lines in optically pumped alkali vapors *Phys. Rev. Lett.* **31** 273–6
- [77] Katz O, Peleg O and Firstenberg O 2015 Coherent coupling of alkali atoms by random collisions *Phys. Rev. Lett.* **115** 113003
- [78] Lukin M D, Fleischhauer M, Zibrov A S, Robinson H G, Velichansky V L, Hollberg L and Scully M O 1997 Spectroscopy in dense coherent media: Line narrowing and interference effects *Phys. Rev. Lett.* **79** 2959–62
- [79] Walker T G and Happer W 1997 Spin-exchange optical pumping of noble-gas nuclei *Rev. Mod. Phys.* **69** 629
- [80] Katz O and Firstenberg O 2018 Light storage for one second in room-temperature alkali vapor *Nat. Commun.* **9** 2074
- [81] Phillips N B, Gorshkov A V and Novikova I 2011 Light storage in an optically thick atomic ensemble under conditions of electromagnetically induced transparency and four-wave mixing *Phys. Rev. A* **83** 063823
- [82] Lauk N, O'Brien C and Fleischhauer M 2013 Fidelity of photon propagation in electromagnetically induced transparency in the presence of four-wave mixing *Phys. Rev. A* **88** 013823
- [83] MacAdam K B, Steinbach A and Wieman C 1992 A narrow band tunable diode laser system with grating feedback and a saturated absorption spectrometer for Cs and Rb *Am. J. Phys.* **60** 1098–111
- [84] Adams C S, Firstenberg O and Hofferberth S 2016 Nonlinear quantum optics mediated by Rydberg interactions *J. Phys. B: At. Mol. Opt. Phys.* **49** 1–16
- [85] Pritchard J D, Adams C S and Shaffer J P 2020 Rydberg atom quantum technologies *J. Phys. B: At. Mol. Opt. Phys.* **53** 1–13
- [86] Marino A M and Stroud C R 2008 Phase-locked laser system for use in atomic coherence experiments *Rev. Sci. Instrum.* **79** 013104
- [87] Appel J, MacRae A and Lvovsky A I 2009 A versatile digital GHz phase lock for external cavity diode lasers *Meas. Sci. Technol.* **20** 055302
- [88] Free space acousto-optic modulators (available at: www.brimrose.com/free-space-ao/acousto-optic-modulators)
- [89] Wong V, Bennink R S, Marino A M, Boyd R W, Stroud C R and Narducci F A 2004 Influence of coherent raman scattering on coherent population trapping in atomic sodium vapor *Phys. Rev. A* **70** 053811
- [90] McCormick C F, Marino A M, Boyer V and Lett P D 2008 Strong low-frequency quantum correlations from a four-wave-mixing amplifier *Phys. Rev. A* **78** 043816

- [91] Novikova I, Phillips N B and Gorshkov A V 2008 Optimal light storage with full pulse-shape control *Phys. Rev. A* **78** 021802
- [92] Lijun M, Slattery O, Kuo P and Tang X 2015 EIT quantum memory with Cs atomic vapor for quantum communication *Proc. SPIE* **9615** 48–55
- [93] Belcher N, Mikhailov E E and Novikova I 2009 Atomic clocks and coherent population trapping: experiments for undergraduate laboratories *Am. J. Phys.* **77** 988–98
- [94] Knappe S, Vishal Shah P D, Schwindt D, Hollberg L, Kitching J, Liew Li-A and Moreland J 2004 A microfabricated atomic clock *Appl. Phys. Lett.* **85** 1460–2
- [95] Peter D D, Schwindt S K, Shah V, Hollberg L, Kitching J, Liew Li-A and Moreland J 2004 Chip-scale atomic magnetometer *Appl. Phys. Lett.* **85** 6409–11
- [96] Long C M and Choquette K D 2008 Optical characterization of a vertical cavity surface emitting laser for a coherent population trapping frequency reference *J. Appl. Phys.* **103** 033101
- [97] Abel R P, Mohapatra A K, Bason M G, Pritchard J D, Weatherill K J, Raitzsch U and Adams C S 2009 Laser frequency stabilization to excited state transitions using electromagnetically induced transparency in a cascade system *Appl. Phys. Lett.* **94** 071107
- [98] Msquared, ni, and mw tunable laser sources (available at: www.m2lasers.com/lasers.html)
- [99] Strekalov D V, Matsko A B and Yu N 2007 Electromagnetically induced transparency with a partially standing drive field *Phys. Rev. A* **76** 053828
- [100] Wynands R and Nagel A 1999 Precision spectroscopy with coherent dark states *Appl. Phys. B* **68** 1
- [101] Seltzer S J et al 2010 Investigation of antirelaxation coatings for alkali-metal vapor cells using surface science techniques *J. Chem. Phys.* **133** 144703
- [102] Seltzer S J and Romalis M V 2009 High-temperature alkali vapor cells with antirelaxation surface coatings *J. Appl. Phys.* **106** 114905
- [103] Daniel A Steck 2010 Alkali d line data (available at: <http://steck.us/alkalidata>)
- [104] Matsko A B, Novikova I, Scully M O and Welch G R 2001 Radiation trapping in coherent media *Phys. Rev. Lett.* **87** 133601
- [105] Cash P, Krzewick W, Paul Machado K, Overstreet R, Silveira M, Stanczyk M, Taylor D and Zhang X 2018 Microsemi chip scale atomic clock (CSAC) technical status, applications and future plans *2018 European Frequency and Time Forum (EFTF)* pp 65–71
- [106] Scully M O and Fleischhauer M 1992 Quantum sensitivity limits of an optical magnetometer based on atomic phase coherence *Phys. Rev. Lett.* **69** 1360–3
- [107] Stahler M, Knappe S, Affolderbach C, Kemp W and Wynands R 2001 Picotesla magnetometry with coherent dark states *Europhys. Lett.* **54** 323–8
- [108] Yudin V I, Taichenachev A V, Dudin Y O, Velichansky V L, Zibrov A S and Zibrov S A 2010 Vector magnetometry based on electromagnetically induced transparency in linearly polarized light *Phys. Rev. A* **82** 033807
- [109] Kevin Cox V I, Yudin A V, Taichenachev I N and Mikhailov E E 2011 Measurements of the magnetic field vector using multiple electromagnetically induced transparency resonances in Rb vapor *Phys. Rev. A* **83** 015801
- [110] Deng K, Guo T, He D W, Liu X Y, Liu L, Guo D Z, Chen X Z and Wang Z 2008 Effect of buffer gas ratios on the relationship between cell temperature and frequency shifts of the coherent population trapping resonance *Appl. Phys. Lett.* **92** 211104
- [111] Zanon T, Guérandel S, de Clercq E, Holleville D, Dimarcq N and Clairon A 2005 High contrast Ramsey fringes with coherent-population-trapping pulses in a double lambda atomic system *Phys. Rev. Lett.* **94** 193002
- [112] Liu X, Mérola J-M, Guérandel S, de Clercq E and Boudot R 2013 Ramsey spectroscopy of high-contrast CPT resonances with push-pull optical pumping in cs vapor *Opt. Express* **21** 12451–9
- [113] Mohapatra A K, Bason M G, Butscher B, Weatherill K J and Adams C S 2008 A giant electro-optic effect using polarizable dark states *Nat. Phys.* **4** 890–4
- [114] Sedlacek J A, Schwettmann A, Kübler H, Löw R, Pfau T and Shaffer J P 2012 Microwave electrometry with Rydberg atoms in a vapour cell using bright atomic resonances *Nat. Phys.* **8** 819–24
- [115] Gordon J A, Simons M T, Haddab A H and Holloway C L 2019 Weak electric-field detection with sub-1 Hz resolution at radio frequencies using a Rydberg atom-based mixer *AIP Adv.* **9** 045030
- [116] Jau Y-Y and Carter T 2020 Vapor-cell-based atomic electrometry for detection frequencies below 1 kHz *Phys. Rev. Appl.* **13** 054034
- [117] Fancher C T, Scherer D R, John M C S and Schmittberger Marlow B L 2021 Rydberg atom electric field sensors for communications and sensing *IEEE Trans. Quantum Eng.* **2** 1–13
- [118] Cox K C, Meyer D H, Fatemi F K and Kunz P D 2018 Quantum-limited atomic receiver in the electrically small regime *Phys. Rev. Lett.* **121** 110502
- [119] Prajapati N, Rotunno A, Berweger S, Simons M, Artusio-Glimpse A and Holloway C L 2022 Tv and video game streaming with a quantum receiver: A study on a Rydberg atom-based receivers bandwidth and reception clarity (arXiv:2205.02716)
- [120] Meyer D H, Kunz P D and Cox K C 2021 Waveguide-coupled Rydberg spectrum analyzer from 0 to 20 GHz *Phys. Rev. Appl.* **15** 014053
- [121] Holloway C L, Simons M T, Gordon J A, Dienstfrey A, Anderson D A and Raithel G 2017 Electric field metrology for si traceability: Systematic measurement uncertainties in electromagnetically induced transparency in atomic vapor *J. Appl. Phys.* **121** 233106
- [122] Hsiao Y-F, Tsai P-J, Chen H-S, Lin S-X, Hung C-C, Lee C-H, Chen Y-H, Chen Y-F, Yu I A and Chen Y-C 2018 Highly efficient coherent optical memory based on electromagnetically induced transparency *Phys. Rev. Lett.* **120** 183602
- [123] Finkelstein R, Poem E, Michel O, Lahad O and Firstenberg O 2018 Fast, noise-free memory for photon synchronization at room temperature *Sci. Adv.* **4** 1
- [124] Davidson O, Yogev O, Poem E, and Firstenberg O 2022 Fast, noise-free atomic optical memory with 35% end-to-end efficiency (arXiv:2212.04263)
- [125] Wang Y, Craddock A, Sekelsky R, Flament M and Namazi M 2022 A room-temperature field-deployable quantum memory for quantum repeater schemes *Proc. SPIE* **12015** 38–42
- [126] Firstenberg O, Peyronel T, Liang Q, Gorshkov A V, Lukin M D and Vuletic V 2013 Attractive photons in a quantum nonlinear medium *Nature* **502** 71–75
- [127] Gorniaczyk H, Tresp C, Schmidt J, Fedder H and Hofferberth S 2014 Single-photon transistor mediated by interstate Rydberg interactions *Phys. Rev. Lett.* **113** 053601
- [128] Lahad O and Firstenberg O 2017 Induced cavities for photonic quantum gates *Phys. Rev. Lett.* **119** 113601
- [129] Tiarks D, Schmidt-Eberle S, Stolz T, Rempe G and Dürr S 2019 A photon–photon quantum gate based on Rydberg interactions *Nat. Phys.* **15** 124–6

- [130] Mikhailov E E, Goda K, Corbitt T and Mavalvala N 2006 Frequency-dependent squeeze-amplitude attenuation and squeeze-angle rotation by electromagnetically induced transparency for gravitational-wave interferometers *Phys. Rev. A* **73** 053810
- [131] Keaveney J, Sargsyan A, Sarkisyan D, Papoyan A and Adams C S 2014 Active narrowband filtering, line narrowing and gain using ladder electromagnetically induced transparency in an optically thick atomic vapour *J. Phys. B: At. Mol. Opt. Phys.* **47** 075002
- [132] Akamatsu D, Akiba K and Kozuma M 2004 Electromagnetically induced transparency with squeezed vacuum *Phys. Rev. Lett.* **92** 203602
- [133] Figueroa E, Lobino M, Korystov D, Appel J and Lvovsky A I 2009 Propagation of squeezed vacuum under electromagnetically induced transparency *New J. Phys.* **11** 013044
- [134] Akamatsu D, Yokoi Y, Arikawa M, Nagatsuka S, Tanimura T, Furusawa A and Kozuma M 2007 Ultraslow propagation of squeezed vacuum pulses with electromagnetically induced transparency *Phys. Rev. Lett.* **99** 153602
- [135] Hêtet G, Buchler B C, Glöeckl O, Hsu M T L, Akulshin A M, Bachor H A and Lam P K 2008 Delay of squeezing and entanglement using electromagnetically induced transparency in a vapour cell *Opt. Express* **16** 7369–81
- [136] Appel J, Figueroa E, Korystov D, Lobino M and Lvovsky A I 2008 Quantum memory for squeezed light *Phys. Rev. Lett.* **100** 093602
- [137] Gleb Romanov G, Horrom T, Novikova I and Mikhailov E E 2014 Propagation of a squeezed optical field in a medium with superluminal group velocity *Opt. Lett.* **39** 1093–6
- [138] Lukin M D, Fleischhauer M, Scully M O and Velichansky V L 1998 Intracavity electromagnetically induced transparency *Opt. Lett.* **23** 295–7
- [139] Wang H, Goorskey D J, Burkett W H and Xiao M 2000 Cavity-linewidth narrowing by means of electromagnetically induced transparency *Opt. Lett.* **25** 1732–4
- [140] Cuozzo S L and Mikhailov E E 2019 Dispersion-enhanced tunability of the laser-frequency response to the cavity-length change *Phys. Rev. A* **100** 023846
- [141] Jing M, Ying H, Jie M, Zhang H, Zhang L, Xiao L and Jia S 2020 Atomic superheterodyne receiver based on microwave-dressed rydberg spectroscopy *Nat. Phys.* **16** 911–15
- [142] Efimovskaya A, Lin Y-W and Shkel A M 2017 Origami-like 3-d folded MEMS approach for miniature inertial measurement unit *J. Microelectromech. Syst.* **26** 1030–9
- [143] Overstolz T, Haesler J, Bergonzi G, Pezous A, Clerc P-A, Ischer S, Kaufmann J and Despont M 2014 Wafer scale fabrication of highly integrated rubidium vapor cells *2014 IEEE 27th Int. Conf. Micro Electro Mechanical Systems (MEMS)* pp 552–5
- [144] Kumar S, Fan H, Kübler H, Jahangiri A J and Shaffer J P 2017 Rydberg-atom based radio-frequency electrometry using frequency modulation spectroscopy in room temperature vapor cells *Opt. Express* **25** 8625–37